Glutamine deprivation triggers NAGK-dependent hexosamine salvage

Sydney L. Campbell[1,2], Clementina Mesaros[3], Luke Izzo[1,2], Hayley Affronti[1,2], Michael Noji[1,2], Bethany E. Schaffer[4], Tiffany Tsang[1,2], Kathryn Sun[5], Sophie Trefely[1,2,6], Salisa Kruijning[1,2], John Blenis[4], Ian A. Blair[3], Kathryn E. Wellen[1,2,7]

[1]Department of Cancer Biology, [2]Abramson Family Cancer Research Institute, [3]Department of Systems Pharmacology and Translational Therapeutics, University of Pennsylvania, Philadelphia, PA 19104; [4]Meyer Cancer Center and Department of Pharmacology, Weill Cornell Medicine, New York, NY 10021; [5]Pancreatic Cancer Research Center, Perelman School of Medicine, University of Pennsylvania, Philadelphia, PA 19104; [6]Center for Metabolic Disease Research, Department of Microbiology and Immunology, Lewis Katz School of Medicine, Temple University, Philadelphia, PA 19140. [7]Corresponding author.

Abstract

Tumors frequently exhibit aberrant glycosylation, which can impact cancer progression and therapeutic responses. The hexosamine biosynthesis pathway (HBP) produces uridine diphosphate N-acetylglucosamine (UDP-GlcNAc), a major substrate for glycosylation in the cell. Prior studies have identified the HBP as a promising therapeutic target in pancreatic ductal adenocarcinoma (PDA). The HBP requires both glucose and glutamine for its initiation. The PDA tumor microenvironment is nutrient poor, however, prompting us to investigate how nutrient limitation impacts hexosamine synthesis. Here, we identify that glutamine limitation in PDA cells suppresses de novo hexosamine synthesis but results in increased free GlcNAc abundance. GlcNAc salvage via N-acetylglucosamine kinase (NAGK) is engaged to feed UDP-GlcNAc pools. *NAGK* expression is elevated in human PDA, and *NAGK* deletion from PDA cells

This manuscript has been co-submitted with Kim et al. (2020), “Pancreatic Cancers Scavenge Hyaluronic Acid to Support Growth.”

23 impairs tumor growth in mice. Together, these data identify an important role for NAGK-
24 dependent hexosamine salvage in supporting PDA tumor growth.

25

26 **Introduction**
27

28 Altered glycosylation is frequently observed in malignancies, impacting tumor growth as well
29 as immune and therapeutic responses (Akella et al., 2019; Mereiter et al., 2019; Munkley,
30 2019). Several types of glycosylation, including O-GlcNAcylation and N-linked glycosylation, are
31 dependent on the glycosyl donor uridine diphosphate N-acetylglucosamine (UDP-GlcNAc),
32 which is synthesized by the hexosamine biosynthesis pathway (HBP). The HBP branches off
33 from glycolysis with the transfer of glutamine's amido group to fructose-6-phosphate (F-6-P) to
34 generate glucosamine-6-phosphate (GlcN-6-P), mediated by the rate limiting enzyme
35 glutamine—fructose-6-phosphate transaminase (GFPT1/2). The pathway further requires
36 acetyl-CoA, ATP, and uridine triphosphate (UTP) to ultimately generate UDP-GlcNAc. O-
37 GlcNAcylation, the addition of a single N-acetylglucosamine (GlcNAc) moiety onto a serine or
38 threonine residue of intracellular proteins, is upregulated in multiple cancers (Akella, et al.,
39 2019). Targeting O-GlcNAcylation suppresses the growth of breast, prostate, and colon cancer
40 tumors (Caldwell et al., 2010; Ferrer et al., 2017; Gu et al., 2010; Guo et al., 2017; Lynch et al.,
41 2012). Similarly, highly branched N-glycan structures are sensitive to HBP flux and are
42 upregulated in malignant tissue, and targeting the relevant Golgi GlcNAc transferase enzymes
43 can limit tumor growth and metastasis in vivo (Granovsky et al., 2000; Li et al., 2008; Zhou et
44 al., 2011). Thus, improved understanding the regulation of the HBP in cancer could point
45 towards novel therapeutic strategies.

This manuscript has been co-submitted with Kim et al. (2020), "Pancreatic Cancers Scavenge Hyaluronic Acid to Support Growth."

46 Pancreatic ductal adenocarcinoma (PDA) is a deadly disease with a 5-year survival rate of 9%
47 and a rising number of annual deaths (Rahib et al., 2014) (ACS Cancer Facts and Figures 2019,
48 NIH SEER report 2019). Mutations in *KRAS* occur in nearly all cases of human PDA and drive
49 extensive metabolic reprogramming in cancer cells. Enhanced flux into the HBP was identified
50 as a primary metabolic feature mediated by mutant KRAS in PDA cells (Ying et al., 2012).
51 Hypoxia, a salient characteristic of the tumor microenvironment (Lyssiotis and Kimmelman,
52 2017), was shown to further promote expression of glycolysis and HBP genes in pancreatic
53 cancer cells (Guillaumond et al., 2013). Notably, the glutamine analog 6-diazo-5-oxo-L-
54 norleucine (DON), which inhibits the HBP, suppressed PDA metastasis and sensitized PDA
55 tumors to anti-PD1 therapy (Sharma et al., 2020). DON has also been reported to sensitize PDA
56 cells to the chemotherapeutic gemcitabine in vitro (Chen et al., 2017). Additionally, a recently
57 developed inhibitor targeting the HBP enzyme phosphoacetylglucosamine mutase 3 (PGM3)
58 enhances gemcitabine-mediated reduction of xenograft tumor growth in vivo (Ricciardiello et al.,
59 2020). Thus, the HBP may represent a therapeutic target in PDA, although the regulation of
60 UDP-GlcNAc synthesis and the optimal strategies to target this pathway for therapeutic benefit
61 in PDA remain poorly understood.

62 An outstanding question is the impact of the tumor microenvironment on UDP-GlcNAc
63 synthesis. The HBP has been proposed as a nutrient-sensing pathway since its rate-limiting
64 step, mediated by GFPT1/2, requires both glutamine and the glycolytic intermediate fructose-6-
65 phosphate (Denzel and Antebi, 2015). In hematopoietic cells, glucose deprivation limits UDP-
66 GlcNAc levels and dramatically reduces levels of the N-glycoprotein IL3Rα at the plasma
67 membrane in a manner dependent on the HBP (Wellen et al., 2010). Similarly, O-GlcNAcylation
68 of certain nuclear-cytosolic proteins, including cancer-relevant proteins such as Myc and Snail,
69 has been demonstrated to be nutrient sensitive, impacting protein stability or function (Housley

70 et al., 2008; Park et al., 2010; Swamy et al., 2016). Yet, the PDA tumor microenvironment is
71 thought to be particularly nutrient poor, owing to its characteristic dense stroma (Halbrook and
72 Lyssiotis, 2017). This raises the question of how nutrient deprivation impacts the synthesis of
73 UDP-GlcNAc and its utilization for glycosylation. Understanding how PDA cells regulate these
74 processes under nutrient limitation could identify therapeutic vulnerabilities. In this study, we
75 investigated the impact of nutrient deprivation on the HBP and glycosylation in PDA cells,
76 identifying a key role for hexosamine salvage through the enzyme N-acetylglucosamine kinase
77 (NAGK) in PDA tumor growth.

78 **Materials and methods**

KEY RESOURCES TABLE				
Reagent type (species) or resource	**Designation**	**Source or reference**	**Identifiers**	**Additional information**
cell line (Homo sapiens)	MIA PaCa-2	ATCC	CRL-1420	
cell line (Homo sapiens)	PANC-1	ATCC	CRL-1469	
cell line (Homo sapiens)	HPAC	ATCC	CRL-2119	
cell line (Homo sapiens)	AsPC-1	ATCC	CRL-1682	
cell line (Homo sapiens)	BxPC-3	ATCC	CRL-1687	
cell line (Homo sapiens)	HCT 116	ATCC	CCL-247	

This manuscript has been co-submitted with Kim et al. (2020), “Pancreatic Cancers Scavenge Hyaluronic Acid to Support Growth.”

cell line (Homo sapiens)	SW480	ATCC	CCL-228	
Plasmid	lentiCRISPR v2	Addgene	52961	
Antibody	O-GlcNAc CTD1106	Cell Signaling	9875S	
Antibody	tubulin	Sigma	T6199	
Antibody	HSP60	Cell Signaling	12165S	
Antibody	NAGK	Atlas Antibodies	HPA035207	
Antibody	NAGK	Proteintech	15051-1-AP	
Antibody	AKT phosphoS473	Cell Signaling	4060	
Antibody	Viniculin	Sigma	V9264	
Chemical compound	[U-13C]-glucose	Cambridge Isotopes	CLM-1396-1	
Chemical compound	13C GlcNAc	Omicron Biochemicals	GLC-006	
Strain	NCr nude mice	Taconic	CrTac:NCr-Foxn1nu	
Sequenced-based reagent	*GFPT1* forward	This paper	RT-qPCR primers	CTCTGGCTTTGGTGGATAAA
Sequenced-based reagent	*GFPT1* reverse	This paper	RT-qPCR primers	GCAACCACTTGCTGAAGA
Sequenced-based reagent	*NAGK* forward	This paper	RT-qPCR primers	GTGCTCATATCTGGAACAGG
Sequenced-based reagent	*NAGK* reverse	This paper	RT-qPCR primers	ACCCTCATCACCCATCATA
Sequenced-based reagent	*HPRT* forward	This paper	RT-qPCR primers	ATTATGCCGAGGATTTGGAA
Sequenced-based reagent	*HPRT* reverse	This paper	RT-qPCR primers	CCCATCTCCTTCATGACATCT

This manuscript has been co-submitted with Kim et al. (2020), “Pancreatic Cancers Scavenge Hyaluronic Acid to Support Growth.”

Sequenced-based reagent	*RPL19* forward	This paper	RT-qPCR primers	CAAGAAGGAGGAGATCATCAAG
Sequenced-based reagent	*RPL19* reverse	This paper	RT-qPCR primers	ATCACAGAGGCCAGTATGTA
Sequenced-based reagent	sgMGAT5 mouse forward	Doench et al., 2016	CRISPR deletion primers	CACCGGCTGTCATGACACCAGCGTA
Sequenced-based reagent	sgMGAT5 mouse reverse	Doench et al., 2016	CRISPR deletion primers	AAACTACGCTGGTGTCATGACAGCC
Sequenced-based reagent	sgNAGK#1 forward	Doench et al., 2016	CRISPR deletion primers	CACCGTTGACGTAGCCGATATCATG
Sequenced-based reagent	sgNAGK#1 reverse	Doench et al., 2016	CRISPR deletion primers	AAACCATGATATCGGCTACGTCAAC
Sequenced-based reagent	sgNAGK#2 forward	Doench et al., 2016	CRISPR deletion primers	CACCGTGCTTGGTGTGCGATCCAGT
Sequenced-based reagent	sgNAGK#2 reverse	Doench et al., 2016	CRISPR deletion primers	AAACACTGGATCGCACACCAAGCAC
Sequenced-based reagent	sgNAGK#3 forward	Doench et al., 2016	CRISPR deletion primers	CACCGCTCTACACCCCCATAGATCG
Sequenced-based reagent	sgNAGK#3 reverse	Doench et al., 2016	CRISPR deletion primers	AAACCGATCTATGGGGGTGTAGAGC
Sequenced-based reagent	siRNA non-targeting control	Santa Cruz Biotechnology	SC-37007	
Sequenced-based reagent	siGALE	Santa Cruz Biotechnology	SC-78950	
Sequenced-based reagent	siGNE	Santa Cruz Biotechnology	SC-60693	

This manuscript has been co-submitted with Kim et al. (2020), “Pancreatic Cancers Scavenge Hyaluronic Acid to Support Growth.”

Sequenced-based reagent	siGALK2	Santa Cruz Biotechnology	SC-90002	

79

80

81 **Cell culture**

82 Cells were cultured in DMEM high glucose (Gibco, 11965084) with 10% calf serum (Gemini
83 GemCell U.S. Origin Super Calf Serum, 100-510), unless otherwise noted. Glucose- or
84 glutamine-restricted media was prepared using glucose, glutamine, and phenol red free DMEM
85 (Gibco, A1443001) supplemented with glucose (Sigma-Aldrich, G8769), glutamine (Gibco,
86 25030081), and dialyzed fetal bovine serum (Gemini, 100-108). For all glutamine restriction
87 experiments except S2.3 D, cells were plated 2-3x more densely for the nutrient restricted
88 condition samples to achieve similar confluency at the experiment endpoint. 1% oxygen levels
89 were achieved by culturing cells in a Whitley H35 Hypoxystation (Don Whitley Scientific). ATCC
90 names and numbers for the cell lines used in this study are: MIA PaCa-2 (ATCC# CRL-1420),
91 PANC-1 (ATCC# CRL-1469), HPAC (ATCC# CRL-2119), AsPC-1 (ATCC# CRL-1682), BxPC-3
92 (ATCC# CRL-1687), HCT 116 (ATCC# CCL-247), and SW480 (ATCC# CCL-228). All cells were
93 routinely tested for mycoplasma and authenticated by short tandem repeat (STR) profiling using
94 the GenePrint 10 System (Promega, B9510).

95 **Generation of CRISPR cell lines**

96 sgRNA sequences targeting *NAGK* or *Mgat5* from the Brunello and Brie libraries (Doench et al.,
97 2016) were cloned into the lentiCRISPRv2 vector (Sanjana, Shalem et al., 2014). Lentivirus was
98 produced in 293T cells according to standard protocol. Cells were then infected with the
99 CRISPR lentivirus and selected with puromycin. Cells were plated at very low density into 96

100 well plates to establish colonies generated from single cell clones. *Mgat5* gene disruption was
101 validated by qPCR and L-PHA binding. *NAGK* gene disruption was validated by qPCR, western
102 blot, and ^{13}C-GlcNAc tracing. Seven *NAGK* knockout clonal cell lines established from three
103 different sgRNAs, four in PANC-1 cells and three in MIA PaCa-2 cells, were chosen for use in
104 the study. Please see table at end of methods for primer sequences of guides used.

105 **Western blotting**

106 For protein extraction from cells, cells were kept on ice and washed three times with PBS, then
107 scraped into PBS and spun down at 200g for 5 minutes. The cell pellet was resuspended in 50-
108 100 µL RIPA buffer [1% NP-40, 0.5% deoxycholate, 0.1% SDS, 150 mM NaCl, 50 mM Tris plus
109 protease inhibitor cocktail (Sigma-Aldrich, P8340) and phosSTOP (Sigma-Aldrich,
110 04906845001)] and lysis was allowed to continue on ice for 10 minutes. Cells were sonicated
111 with a Fisherbrand Model 120 Sonic Dismembrator (Fisher Scientific, FB120A110) for three
112 pulses of 20 seconds each at 20% amplitude. Cell lysate was spun down at 15,000g for 10
113 minutes at 4°C and supernatant was transferred to a new tube. For protein extraction from
114 tissue, the sample was resuspended in 500 µL RIPA buffer and homogenized using a
115 TissueLyser (Qiagen, 85210) twice for 30s at 20 Hz. Following incubation on ice for 10 minutes
116 the same procedure was followed as for cells. For both cells and tissue, lysate samples were
117 stored at -80°C until analysis by immunoblot. All blots were developed using a LI-COR Odyssey
118 CLx system. Antibodies used in this study were: O-GlcNAc CTD110.6 (Cell Signaling 9875S),
119 tubulin (Sigma T6199), HSP60 (Cell Signaling 12165S), NAGK (Atlas Antibodies, HPA035207),
120 and PARP (Cell Signaling 9532).

121 For blots showing the mobility shift for NAGK in low glutamine, samples were prepared in lysis
122 buffer containing 50 mM Tris pH 8.0, 150 mM NaCl, 0.5% IGEPAL CA-630 (Sigma, I3021), 1

123 mM PMSF, 1.5 μM aprotinin, 84 μM leupeptin, 1 μM pepstatin A, -/+ 10 mM NaF and 20 mM
124 Na_3VO_4 as indicated. To visualize the NAGK mobility shift in response to low glutamine, 20 μg
125 total protein per sample was separated across 12.5 cm of 11% SDS-PAGE resolving space
126 under reducing conditions using the large electrophoresis systems available from C.B.S.
127 Scientific until approximately 3 cm of separation was obtained between the 25 and 37 kDa
128 protein standards (Bio-Rad; 1610375). Using electrophoresis, proteins were transferred (30 V,
129 4°C, overnight) to 0.45 uM pore size nitrocellulose membrane (Amersham, 10600002). The
130 primary antibodies used were NAGK (Proteintech, 15051-1-AP), AKT phosphoS473 (Cell
131 Signaling Technology, 4060), and Vinculin (Sigma, V9264). Membranes were developed using
132 the LI-COR Odyssey CLx system.

133 **RT-qPCR**

134 For RNA extraction from cells, cells were put on ice, washed with PBS, and scraped into PBS.
135 Samples were then spun down at 200g for 5 minutes and resuspended in 100 μL Trizol (Life
136 Technologies). For RNA extraction from tissue, samples were resuspended in 500 μL Trizol and
137 homogenized using a TissueLyser twice for 30s at 20 Hz. For both cells and tissue, RNA was
138 extracted following the Trizol manufacturer protocol. cDNA was prepared using high-capacity
139 RNA-to-cDNA master mix (Applied Biosystems, 4368814) according to kit instructions. cDNA
140 was diluted 1:20 and amplified with PowerUp SYBR Green Master Mix (Applied Biosystems,
141 A25778) using a ViiA-7 Real-Time PCR system. Fold change in expression was calculated by
142 the $\Delta\Delta C_t$ method using HPRT as a control. Please see table at end of chapter for primer
143 sequences.

144 **Lectin binding assay**

145 Cells were put on ice, washed with PBS and then scraped into PBS. Samples were then spun
146 down at 200g for 5 minutes and resuspended in 3% BSA with fluorophore-conjugated lectin
147 added 1:1000 (Vector Labs FL-1111-2). Samples were covered and incubated on ice for 30
148 minutes at room temperature, then spun down and resuspended in PBS before analysis with an
149 Attune NxT Flow Cytometer (Thermo Fisher Scientific). Data was further analyzed using FlowJo
150 8.7.

151 **Metabolite quantitation and labeling**

152 For all metabolite quantitation experiments, each sample was collected from a 10 cm sub-
153 confluent plate of cells. To achieve similar confluency and protein content at the experiment
154 endpoint, cells were initially plated more densely for the nutrient deprived samples than for the
155 nutrient replete samples. For low glutamine experiments, PANC-1 cells were plated $3x10^5$ for 4
156 mM glutamine samples and $5.5x10^5$ for 0.05 mM samples. MIA PaCa-2 cells were plated $3x10^5$
157 for 4 mM samples and $1.2x10^6$ for 0.05 mM samples.

158 Samples were prepared according to Guo et al. (Guo et al., 2016). Briefly, cells were put on ice
159 and washed 3x with PBS. Then, 1 mL of ice cold 80% methanol was added to the plate, and
160 cells were scraped into solvent and transferred to a 1.5 mL tube. For quantitation experiments,
161 internal standard containing a mix of ^{13}C labeled metabolites was added at this time. Samples
162 were then sonicated and spun down, and the supernatants were dried down under nitrogen.
163 The dried samples were then resuspended in 100 µL of 5% sulfosalicylic acid and analyzed by
164 liquid chromatography-high resolution mass spectrometry as reported (Guo et al., 2016) with the
165 only modification that the LC was coupled to a Q Exactive-HF with a heated ESI source
166 operating in negative ion mode alternating full scan and MS/MS modes. The $[M-H]^-$ ion of each
167 analyte and its internal standard was quantified, with peak confirmation by MS/MS. GlcNAc

168 quantification was done on a triple quadropole instrument exactly as described (Guo et al.,
169 2016). Data analysis was conducted in Thermo XCalibur 3.0 Quan Browser and FluxFix (Trefely
170 et al., 2016). For quantitation experiments, samples were normalized first to peak integrations of
171 ^{13}C-labeled internal standard components and then to protein content in the sample, measured
172 by BCA assay. Relative quantification was then calculated by normalizing to the control
173 condition in each experiment.

174 For glucose labeling experiments, cells were cultured in DMEM without glucose, glutamine, or
175 phenol red supplemented with 10 mM [U-^{13}C]-glucose (Cambridge Isotopes, CLM-1396-1), 4
176 mM glutamine, and 10% dialyzed fetal bovine serum. Cells were incubated for the indicated
177 time, and samples were prepared as above. For GlcNAc labeling experiments, cells were
178 cultured in DMEM without glucose, glutamine, or phenol red supplemented with 10 mM N-[1,2-
179 13C2]acetyl-D-glucosamine (^{13}C GlcNAc) (Omicron Biochemicals, GLC-006), 4 mM glutamine,
180 10 mM glucose, and 10% dialyzed fetal bovine serum. Cells were incubated for the indicated
181 time, and samples were prepared as above.

182 **Soft agar colony formation assay**

183 Cells were trypsinized and counted using a Bright-Line hemacytometer (Sigma, Z359629). The
184 bottom agar layer was prepared by adding Bacto Agar (BD Bioscience, 214050) to cell culture
185 media for a final concentration of 0.6%. 2 mL bottom agar was added to each well of a 6-well
186 tissue culture plate. Once bottom agar solidified, top layer agar was prepared by combining
187 trypsinized cells with the bottom agar mix for a final concentration of 0.3% Bacto Agar. 1 mL top
188 layer agar was added to each well with a bottom layer of agar. Cells were plated 2.5×10^4 per
189 well. 0.5 mL DMEM high glucose with 10% calf serum was added to cells every 7 days. Images

190 were taken after 3 weeks. Images were blinded and colonies per image were counted using
191 ImageJ (Schneider et al., 2012).

192 **2D Proliferation assay**

193 Cells were plated $3.5x10^4$ per well of a 6-well plate. For each day that counts were recorded,
194 three wells were trypsinized and cells were counted twice using a hemocytometer (Sigma,
195 Z359629). The average of the two counts was recorded for each well, and the average count of
196 the three wells was used to graph the data. For proliferation assays in 0.05 mM glutamine,
197 trypan blue was used during cell counts.

198 **Bioinformatics data analysis**

199 The PDAC expression profiling dataset (GEO accession GSE16515, Pei et al., 2009) from NCBI
200 GEO Profile database (Edgar et al., 2002) was used to compare the expression level between
201 human normal and PDAC tumor samples. The dataset consists of 52 samples, in which 16
202 samples are matched tumor and normal tissues, and 20 samples are only tumor tissues. The
203 statistical analysis was conducted by one-way ANOVA, the level of significance was evaluated
204 by $p < 0.01$ and plotted in box-and-whisker diagram. Comparison of HBP gene expression
205 between tumor (TCGA PAAD dataset) and normal tissue (GTEx) was also conducted using
206 GEPIA2 (Tang et al., 2019).

207 **Tumor growth in vivo**

208 $3x10^6$ PANC-1 NAGK CRISPR cells were injected with 1:1 Matrigel (Corning, CB354248) into
209 the flanks of NCr nude mice and measured with calipers once per week for 22 weeks. At the
210 experiment endpoint (22 weeks or when tumor reached 20 mm in length), mice were euthanized
211 with CO_2 and cervical dislocation. Tumors were removed, weighed, cut into pieces for analysis,

212 and frozen. All animal experiments were approved by the University of Pennsylvania and the
213 Institutional Animal Care and Use Committee (IACUC).

214

215 **Results**

216

217 **Tetra-antennary N-glycans and O-GlcNAcylation are minimally impacted by nutrient**
218 **limitation in pancreatic cancer cells**

219 To examine the effects of nutrient deprivation on glycosylation, we cultured cells under
220 glucose or glutamine limitation and examined O-GlcNAc levels and cell surface
221 phytohemagglutinin-L (L-PHA) binding, a readout of N-acetylglucosaminyltransferase 5
222 (MGAT5)-mediated cell surface N-glycans (Fig S1A, B), which are highly sensitive to UDP-
223 GlcNAc availability (Lau et al., 2007). We focused on glucose and glutamine because of their
224 requirement to initiate the HBP (Fig. 1A). First, as a positive control, we examined HCT-116 and
225 SW480 colon cancer cells, previously documented to have glucose-responsive O-GlcNAcylation
226 (Park et al., 2010; Steenackers et al., 2016), which we also confirmed in HCT-116 cells (Fig.
227 1B). Indeed, L-PHA binding was suppressed by glucose restriction in SW480 cells and by
228 glutamine restriction in both colon cancer cell lines (Fig. 1C). Next, to test whether glycans were
229 sensitive to nutrient restriction in PDA cells, we examined L-PHA binding and O-GlcNAc levels
230 under nutrient deprivation conditions in a panel of human PDA cell lines, including PANC-1, MIA
231 PaCa-2, AsPC-1, and HPAC. Across these cell lines, no consistent changes in L-PHA binding
232 were observed under glucose or glutamine limitation (Fig. 1D, E; Fig. S1C). We also examined
233 L-PHA binding in PDA cells under oxygen- or serum-deprived conditions and observed minimal
234 changes (Figure S1D, E). O-GlcNAcylation was minimally altered by culture in low glutamine
235 and exhibited variable changes in response to glucose limitation (Fig. 1F), consistent with

236

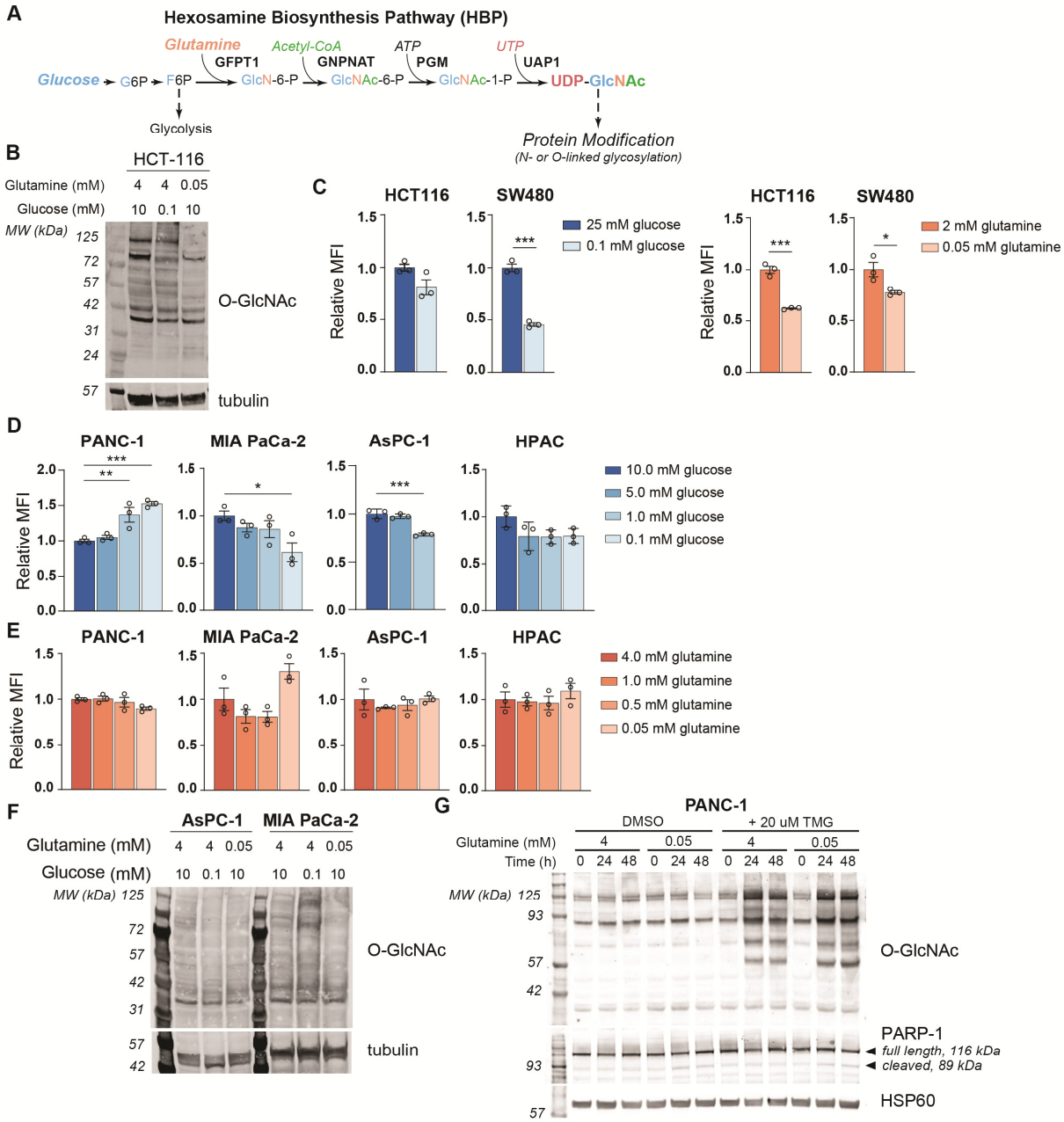

Figure 1: MGAT5-dependent N-glycans are minimally impacted by glucose or glutamine deprivation in PDA cells.
A) Overview of the hexosamine biosynthesis pathway (HBP). **B)** O-GlcNAc levels in HCT-116 cells in high and low nutrients; cells were incubated in indicated concentrations of glucose and glutamine for 48 hours. **C)** Phytohemagglutinin-L (LPHA) binding in colon cancer cells. Cells were incubated in the indicated concentrations of glucose (left) or glutamine (right) for 48 hours and then analyzed by flow cytometry. Graph shows mean fluorescence intensity (MFI) relative to control condition. Statistical significance was calculated by unpaired t-test. **D-E)** Phytohemagglutinin-L (LPHA) binding in pancreatic ductal adenocarcinoma (PDA) cells in low nutrients. Cells were incubated in the indicated concentrations of glucose (D) or glutamine (E) for 48 hours and then analyzed by flow cytometry. Statistical significance was calculated by one-way ANOVA. **F)** O-GlcNAc levels in PDA cells in high and low nutrients. Cells were incubated in the indicated concentrations of glucose or glutamine for 48 hours. **G)** Western blot for O-GlcNAc and PARP in PANC-1 cells cultured in the indicated concentrations of glutamine with or without Thiamet-G (TMG) treatment for the indicated time. For all bar graphs, mean +/- standard error of the mean (SEM) of three biological triplicates is represented. Panels B) - G) are representative of at least two independent experimental replicates. *, $p \leq 0.05$; **, $p \leq 0.01$; ***, $p \leq 0.001$.

This manuscript has been co-submitted with Kim et al. (2020), “Pancreatic Cancers Scavenge Hyaluronic Acid to Support Growth.”

239 stress-induced regulation of this modification (Taylor et al., 2008). Since glycosylation may be
240 maintained through either sustained ability to add the modifications or through changes in
241 turnover, we assayed active O-GlcNAcylation by inhibiting O-GlcNAcase with Thiamet G (TMG).
242 TMG treatment resulted in equivalently elevated O-GlcNAcylation levels in high and low
243 glutamine conditions (Fig. 1G; Fig. S1F), indicating that glutamine restriction does not limit the
244 capacity of cells to add the O-GlcNAc modification. Mia-PaCa-2 cells exhibited some cell death
245 in low glutamine, though this was not exacerbated by TMG treatment (Fig. S1F). Thus, under a
246 variety of nutrient stress conditions, neither L-PHA binding nor O-GlcNAcylation were
247 consistently suppressed in pancreatic cancer cell lines. Glutamine restriction in particular had
248 remarkably little impact on O-GlcNAcylation and L-PHA binding, raising the question of how
249 UDP-GlcNAc is generated during nutrient limitation.
250
251 **De novo UDP-GlcNAc synthesis is suppressed upon glutamine limitation**
252 We therefore next asked whether the abundance of HBP metabolites is impacted by nutrient
253 limitation. We measured HBP metabolites after glucose or glutamine restriction using HPLC-MS
254 (Guo et al., 2016). In low glutamine conditions, GlcN-6-P levels were potently decreased relative
255 to glutamine replete conditions in PANC-1 cells, while UDP-GlcNAc abundance was maintained
256 (Fig. 2A). In MIA PaCa-2 cells, UDP-GlcNAc abundance actually increased upon glutamine
257 restriction (Fig S2.1A). These data indicate that UDP-GlcNAc might be generated through
258 mechanisms other than de novo synthesis. Glycolytic intermediates were minimally impacted by
259 low glutamine conditions, and TCA cycle intermediates such as α-KG and malate decreased as
260 expected (Fig. 2A, Fig. S2.1A). In contrast to that in glutamine restriction, UDP-GlcNAc
261 abundance declined in 5 mM or 0.1 mM relative to 10 mM glucose conditions (Fig. S2.1B),
262

This manuscript has been co-submitted with Kim et al. (2020), "Pancreatic Cancers Scavenge Hyaluronic Acid to Support Growth."

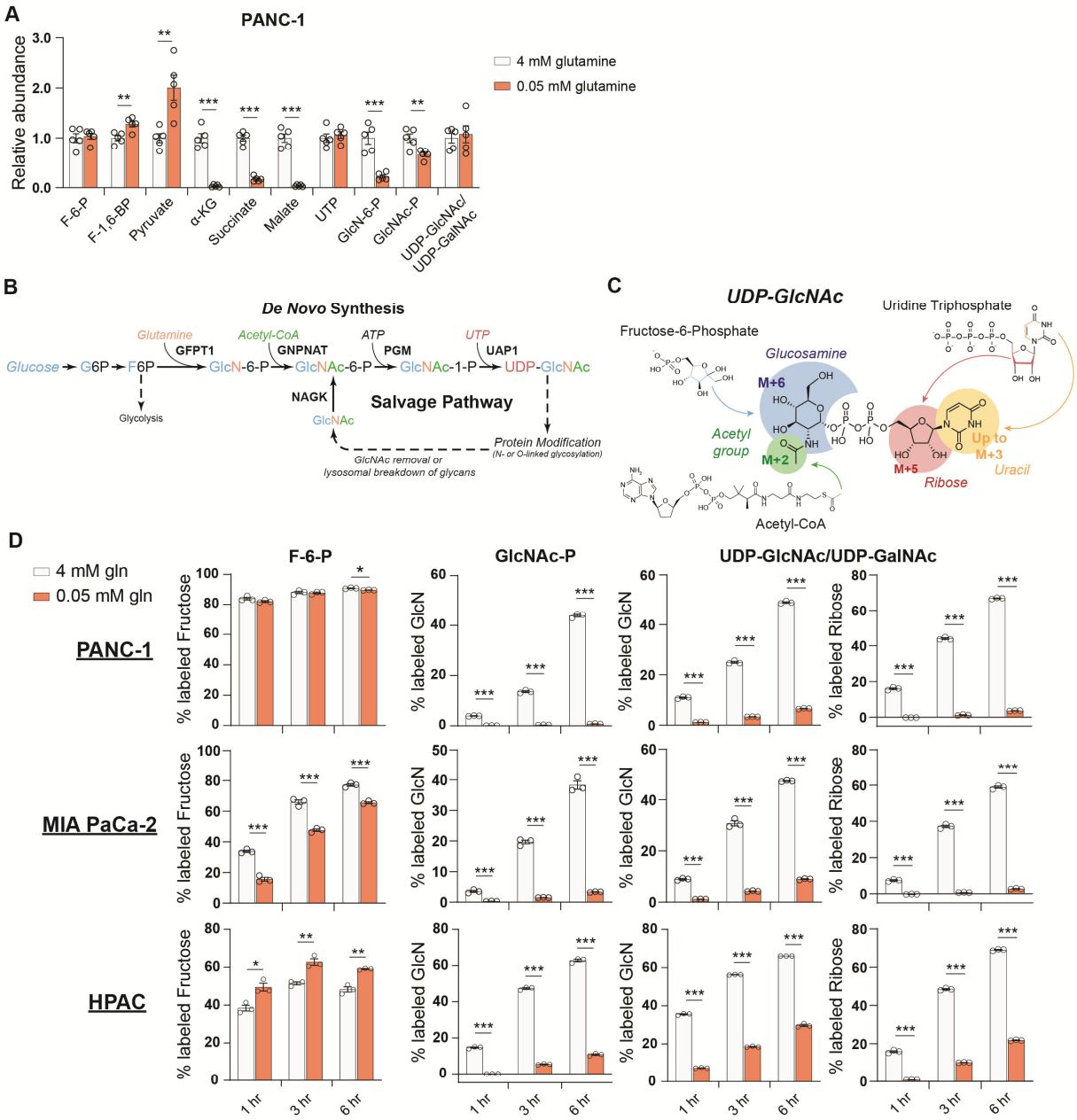

Figure 2: *De novo* UDP-GlcNAc synthesis is supressed upon glutamine limitation.
A) Metabolite measurements in PANC-1 and MIA PaCa-2 cells after culture for 48 hours in 0.05 mM glutamine. Quantification is normalized to 4 mM glutamine condition. Statistical significance was calculated by unpaired t-test.Mean +/- SEM is represented. **B)** Overview of the GlcNAc salvage pathway feeding into the HBP. GlcNAc scavenged from O-GlcNAc removal or lysosomal breakdown of glycans can be phosphorylated by NAGK and used to regenerate UDP-GlcNAc. **C)** Overview of the incorporation of ^{13}C glucose into UDP-GlcNAc. Different parts of the molecule can be labeled from glucose-derived subunits, thus isotopologues up to M+16 can be derived from glucose. **D)** ^{13}C glucose tracing into F-6-P, GlcNAc-P, and UDP-GlcNAc in indicated glutamine concentrations. % labeled GlcN indicates sum of M+6 and M+8 isotopologues for GlcNAc-P and sum of M+6, M+8, M+11, and M+13 for UDP-GlcNAc, % labeled Ribose indicates sum of M+5, M+7, M+11, and M+13 for UDP-GlcNAc. All isotopologues are graphed in Figure S2. Statistical significance was calculated by unpaired t-test. Mean +/- SEM is represented. *, $p \leq 0.05$; **, $p \leq 0.01$; ***, $p \leq 0.001$.

This manuscript has been co-submitted with Kim et al. (2020), “Pancreatic Cancers Scavenge Hyaluronic Acid to Support Growth.”

265 suggesting that glutamine limitation specifically may trigger an adaptive response to sustain
266 UDP-GlcNAc pools.

267 We sought to understand how UDP-GlcNAc pools are sustained during glutamine restriction.
268 In addition to de novo synthesis of UDP-GlcNAc via the HBP, free GlcNAc in the cell can also
269 be phosphorylated via N-acetylglucosamine kinase (NAGK) to produce GlcNAc-P and then
270 regenerate UDP-GlcNAc (Fig. 2B). However, NAGK's roles in physiology and cancer biology
271 have been minimally studied. To investigate the possibility that UDP-GlcNAc is generated
272 through mechanisms other than its synthesis from glucose, we first designed a stable isotope
273 labeling strategy to quantify the fraction of the glucosamine ring that is synthesized *de novo* in
274 glutamine-replete versus -restricted conditions. Since multiple components of UDP-GlcNAc
275 [glucosamine ring, acetyl group, uridine (both the uracil nucleobase and the ribose ring)] can be
276 synthesized from glucose, UDP-GlcNAc isotopologues up to M+16 can be generated from
277 glucose (Moseley et al., 2011) (Fig. 2C). In order to measure the glucose carbon incorporated
278 into GlcNAc-P and UDP-GlcNAc via the HBP, all isotopologues containing a fully labeled
279 glucosamine ring are added together (% labeled GlcN indicates sum of M+6, M+8, M+11, and
280 M+13 for UDP-GlcNAc and sum of M+6 and M+8 for GlcNAc-P) (Fig. 2C).

281 After 48 hours of glutamine restriction, cells were incubated with fresh low glutamine medium
282 containing [U-^{13}C]-glucose to track the incorporation of glucose carbons into hexosamine
283 intermediates. Across multiple PDA cell lines, the fractional labeling of the glucosamine ring in
284 both GlcNAc-P and UDP-GlcNAc pools was markedly suppressed by glutamine restriction,
285 indicating decreased de novo synthesis in low glutamine conditions (Fig. 2D, Fig. S2.1C-E).
286 Notably, labeling into the ribose component of UDP-GlcNAc was also suppressed [% labeled
287 ribose indicates sum of isotopologues containing M+5 (i.e., M+5, M+7, M+11, and M+13); Fig.

288 2D, Fig. S2.1C]. Consistently, incorporation of ^{13}C glucose into uridine triphosphate (UTP) was
289 suppressed upon glutamine restriction (Fig. S2.2A), even though UTP levels were maintained or
290 increased (Fig. 2A, Fig. S2.1A), suggesting a role for nucleoside salvage in maintaining
291 nucleotide pool in these conditions. This is consistent with previous reports demonstrating that
292 autophagy/ ribophagy is a source of nucleosides in amino acid deprived conditions (Guo et al.,
293 2011; Wyant et al., 2018). Indeed, silencing of either of the uridine salvage enzymes uridine
294 kinase 1 or 2 (UCK1/2) resulted in decreased UDP, UTP, and UDP-GlcNAc levels (Fig. S2.2B-
295 C), indicating that nucleoside salvage contributes to maintaining uridine phosphate and UDP-
296 GlcNAc pools.Thus, glutamine restriction suppresses the *de novo* synthesis of both GlcNAc-P
297 and UTP, both of which are required to produce UDP-GlcNAc.

298 We noted that GlcNAc-P and UDP-GlcNAc pools labeled from glucose with similar but not
299 identical kinetics. While this is potentially due to limitations in detection since GlcNAc-P is much
300 less abundant than UDP-GlcNAc, we considered whether GlcNAc-P-independent pathways
301 may also have minor contributions to glucose-dependent UDP-GlcNAc labeling. Although
302 pathways through which glucose can feed into UDP-GlcNAc's glucosamine ring independent of
303 the HBP have not been described in mammalian cells to our knowledge, we nevertheless tested
304 the two major metabolic branch points diverging from UDP-GlcNAc, which mediate UDP-
305 GalNAc and sialic acid synthesis. UDP-galactose-4-epimerase (GALE) interconverts UDP-
306 GlcNAc and UDP-GalNAc, and UDP-GlcNAc-2-epimerase/ManAc kinase (GNE) initiates sialic
307 acid biosynthesis. Silencing of neither GALE nor GNE reduced UDP-GlcNAc labeling from
308 glucose, however, indicating that these enzymes are unlikely to facilitate a bypass pathway (Fig.
309 S2.2D-E). Although a minor contribution from another unknown pathway cannot be ruled out,
310 the slight apparent differences in timing of GlcNAc-P and UDP-GlcNAc labeling most likely

311 reflect technical limitations. Regardless, the data clearly indicate that UDP-GlcNAc abundance
312 is maintained despite reduced *de novo* hexosamine synthesis from glucose (Fig. 2D).

313 **GlcNAc salvage feeds UDP-GlcNAc pools in pancreatic cancer cells**

314 As mentioned, UDP-GlcNAc can be generated via phosphorylation of free GlcNAc by NAGK
315 generating GlcNAc-6-P (Fig. 2B). When supplemented, GlcNAc is salvaged into the UDP-
316 GlcNAc pool (Ryczko et al., 2016; Wellen et al., 2010). Endogenous sources of GlcNAc may
317 include removal of O-GlcNAc protein modifications or breakdown of glycoconjugates and
318 extracellular matrix components. Notably, intracellular levels of GlcNAc increase upon glutamine
319 restriction (Fig. 3A). Yet, the significance of GlcNAc salvage to maintenance of UDP-GlcNAc
320 pools has been little studied, and the proportion of UDP-GlcNAc generated via the NAGK-
321 dependent salvage pathway is unknown.

322 *NAGK* mRNA expression increased in PDA cell lines in low glutamine conditions, and in some
323 cell lines also in low glucose (Fig. S2.3A, B). *GFPT1* expression was also induced in both low
324 glucose conditions, consistent with a prior report (Moloughney et al., 2016), and in low
325 glutamine conditions (Fig. S2.3A), even though *de novo* synthesis is suppressed when
326 glutamine is limited. Protein levels of NAGK did not increase in concordance with mRNA at
327 these time points, however, although a mobility shift potentially indicative of post-translational
328 modification was apparent when protein lysates were run on a gel using a large electrophoresis
329 system (see methods; Fig S2.3C-D). Removal of the phosphatase inhibitor Na_3VO_4 from the
330 sample buffer prevented the mobility shift, suggesting that NAGK may be phosphorylated on
331 one or more residues in low glutamine conditions (Fig. S2.3D). Taken together, these data
332 indicate that under low glutamine conditions, GlcNAc availability for salvage increases and the
333 salvage enzyme NAGK is subject to regulation.

334 This manuscript has been co-submitted with Kim et al. (2020), "Pancreatic Cancers Scavenge Hyaluronic Acid to Support Growth."

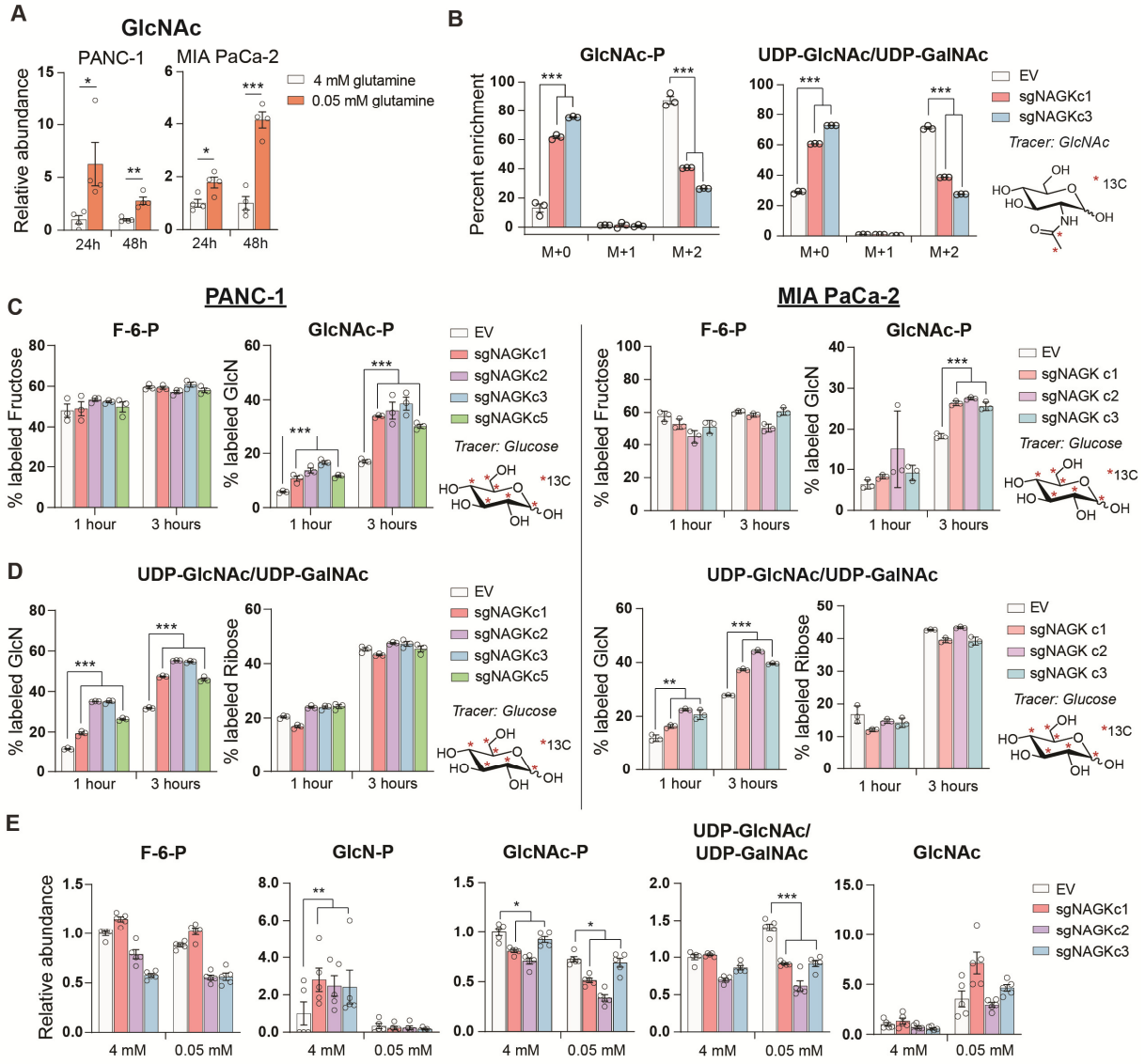

Figure 3: GlcNAc salvage feeds UDP-GlcNAc pools in pancreatic cancer cells.
A) Measurement of GlcNAc in PANC-1 and MIA PaCa-2 cells after incubation in the indicated concentrations of glutamine for 24 and 48 hours. Mean +/- SEM of four biological replicates is represented. Statistical significance was calculated by unpaired t-test. **B)** Measurement of 13C GlcNAc labeled on the acetyl group into GlcNAc-P and UDP-GlcNAc in NAGK knockout cells. Cells were incubated with 10 mM 13C GlcNAc for 6 hours. Mean +/- SEM of three biological replicates is represented. Statistical significance was calculated by unpaired t-test comparing the mean incorporation of the two CRISPR clones and the empty vector (EV) control. **C)** Labeling of F-6-P and GlcNAc-P from 13C glucose in PANC-1 (left) and MIA PaCa-2 (right) NAGK knockout cells. Statistical significance was calculated by unpaired t-test comparing the mean incorporation of the four CRISPR clones and the EV control. Mean +/- SEM of three biological replicates is represented. **D)** Percent of combined UDP-GlcNAc isotopologues containing a labeled glucosamine ring or a labeled ribose from UTP, calculated from S3.1 (E). Statistical significance was calculated by unpaired t-test comparing the mean incorporation of the four CRISPR clones and the EV control. Mean +/- SEM of three biological replicates is represented. **E)** Measurement of HBP metabolites in PANC-1 NAGK knockout cells cultured in the indicated concentrations of glutamine. Statistical significance was calculated by unpaired t-test comparing the mean incorporation of the four CRISPR clones and the EV control. Mean +/- SEM of four biological replicates is represented. *, $p \leq 0.05$; **, $p \leq 0.01$; ***, $p \leq 0.01$.

335

336 This manuscript has been co-submitted with Kim et al. (2020), “Pancreatic Cancers Scavenge Hyaluronic Acid to Support Growth.”

337 These findings prompted us to investigate the role of NAGK in UDP-GlcNAc synthesis in PDA
338 cells. We functionally examined the role of NAGK in PDA cell lines by using CRISPR-Cas9 gene
339 editing to generate NAGK knockout (KO) PANC-1 and MiaPaCa-2 clonal cell lines (Fig. S3.1A-
340 B). N-[1,2-$^{13}C_2$]acetyl-D-glucosamine (^{13}C GlcNAc) was efficiently salvaged in control cells, and
341 this was suppressed by NAGK deletion, as evidenced by reduced fractional labeling of GlcNAc-
342 P and UDP-GlcNAc (Fig. 3B). Since we did not observe any residual protein expression, we
343 hypothesized that the N-acetylgalactosamine (GalNAc) salvage enzyme GalNAc kinase
344 (GALK2) might be responsible for the remaining GlcNAc salvage in the absence of NAGK.
345 Indeed, silencing of GALK2 further suppressed incorporation of ^{13}C GlcNAc into GlcNAc-P and
346 UDP-GlcNAc in the NAGK KO cells (Fig. S3.1C).

347 We hypothesized that knockout cells would conversely conduct increased de novo UDP-
348 GlcNAc synthesis. To test this, we incubated cells with [U-^{13}C]-glucose and examined
349 incorporation into GlcNAc-P and UDP-GlcNAc. Indeed, in the absence of NAGK, we observed
350 increased glucose-dependent fractional labeling of the glucosamine ring of UDP-GlcNAc and
351 GlcNAc-P, but not the ribose component of UDP-GlcNAc (Fig. 3C-D; Fig. S3.1D-E). This effect
352 was also observed with knockdown of NAGK by shRNA, though to a lesser extent (Fig. S3.2A-
353 B). Incorporation of glucose into F-6-P did not change (Fig. 3C) and the proportion of UDP-
354 GlcNAc containing an M+5 ribose ring was also unchanged in knockout cells (Fig. 3D), as
355 expected. Thus, when NAGK is deleted and GlcNAc salvage is suppressed, de novo
356 hexosamine synthesis increases.

357 We next assessed changes in the levels of hexosamine intermediates in control and NAGK
358 KO cell lines. In PANC-1 KO cells in 4 mM glutamine, GlcN-P increased significantly, consistent
359 with increased de novo synthesis in the absence of NAGK (Fig. 3E). GlcNAc-P was modestly

360 reduced in KO cells, though UDP-GlcNAc levels were maintained (Fig. 3E). In MIA PaCa-2
361 cells, GlcNAc-P was markedly suppressed in the absence of NAGK, though UDP-GlcNAc was
362 not (Fig. S3.2C). We also measured HBP metabolites under glutamine restriction, where we
363 expected NAGK would play a more significant role in UDP-GlcNAc generation. We were only
364 able to measure metabolites accurately in PANC-1 KO cells because MIA PaCa-2 NAGK KO
365 cells began to die quickly in low glutamine, which will be discussed further in the next section.
366 GlcN-P decreased in control and KO cells, consistent with reduced de novo hexosamine
367 synthesis (Fig. 3E). GlcNAc-P levels decreased in low glutamine in control cells, and decreased
368 further in cells lacking NAGK, consistent with contributions from both de novo synthesis and
369 salvage (Fig. 3E). Reciprocally, GlcNAc abundance was elevated upon glutamine limitation in
370 both control and NAGK KO cells (Fig. 3E). UDP-GlcNAc abundance was modestly reduced in
371 NAGK KO cells relative to controls under glutamine restriction, though levels were still
372 comparable to that in high glutamine (Fig. 3E), possibly reflecting changes in utilization. GALK2
373 silencing did not further suppress UDP-GlcNAc in NAGK KO cells (Fig. S3.2D), suggesting that
374 GALK2 may not have a major role in physiological GlcNAc salvage. Cumulatively, the data
375 demonstrate that GlcNAc is salvaged into UDP-GlcNAc pools in PDA cells in a manner
376 dependent at least in part on NAGK.

377

378 **NAGK knockout limits tumor growth *in vivo***

379 To test the role of NAGK in cell proliferation, we first monitored growth of NAGK KO cells
380 compared to controls in 2D and 3D culture in 4 mM glutamine, finding minimal differences (Fig.
381 4A, Fig. S4A). We hypothesized that NAGK KO cell proliferation would be impaired in 0.05 mM

382

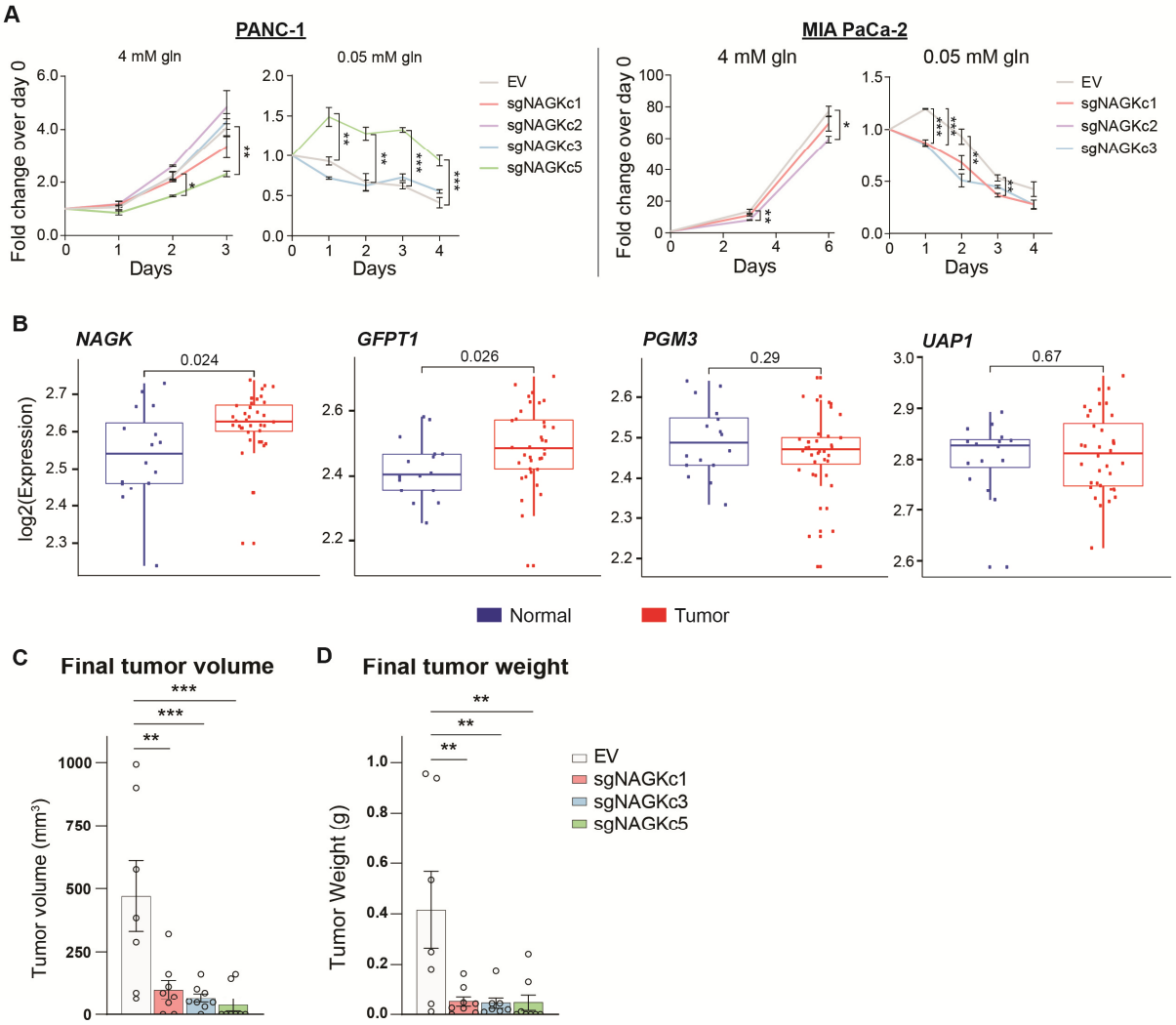

Figure 4: NAGK expression is increased in human PDA tumors and NAGK knockout reduces tumor growth in vivo.
A) 2D proliferation assay by cell count in PANC-1 and MIA PaCa-2 NAGK knockout cells. Mean +/- SEM of three technical replicates is represented. Statistical significance was calculated using one-way ANOVA at each time point. **B)** Gene expression data for NAGK, GFPT1, PGM3, and UAP1 in human PDA tumors compared with matched normal tissue. Statistical analysis was conducted by one-way ANOVA, and level of significance was defined as $p \leq 0.01$. **C)** Final tumor volume and **D)** final tumor weight of subcutaneous tumors generated from PANC-1 NAGK knockout cells in vivo. Cells were injected into the right flank of NCr nude mice and tumor volume was calculated from caliper measurements. Statistical significance was calculated by one-way ANOVA comparing each mean to the EV control mean. Mean +/- SEM of biological replicates is represented (n = 8 each group). *, $p \leq 0.05$; **, $p \leq 0.01$; ***, $p \leq 0.001$.

383

384 This manuscript has been co-submitted with Kim et al. (2020), “Pancreatic Cancers Scavenge Hyaluronic Acid to Support Growth.”

385 glutamine, where *de novo* UDP-GlcNAc synthesis is suppressed. Indeed, MIA PaCa-2 KO cells
386 died more quickly in 0.05 mM glutamine than did control cells (Fig. 4A). PANC-1 KO cells did
387 not show this effect (Fig. 4A), but we hypothesized that NAGK loss might have a stronger effect
388 *in vivo* where tumor growth can be constrained by nutrient availability.

389 To gain initial insight into whether NAGK is likely to play a functional role in PDA progression
390 *in vivo*, we queried publicly available datasets. From analysis of publicly available microarray
391 data (Pei et al., 2009) and gene expression data from the Cancer Genome Atlas (TCGA), we
392 indeed found *NAGK* expression to be increased in tumor tissue relative to adjacent normal
393 regions of the pancreas or to pancreas GTEx data (Fig. 4B, Fig. S4B). *GFPT1* expression was
394 also increased in tumor tissue (Fig. 4B, Fig. S4B), consistent with its regulation by mutant KRAS
395 (Ying et al., 2012). Two other HBP genes, *PGM3* and *UAP1*, did not show significantly
396 increased expression in PDA tumors in these datasets (Fig. 4B, Fig. S4B). We then studied the
397 role of NAGK in tumor growth *in vivo* by injecting NAGK CRISPR KO cells into the flank of NCr
398 nude mice. Final tumor volume and weight were markedly reduced in the absence of NAGK
399 (Fig. 4C-D). Of note, initial tumor growth was comparable between control and KO cells, but the
400 NAGK knockout tumors either stopped growing or shrank while control tumors continued to
401 grow larger (Fig. S4C). Interestingly, KO tumor samples showed increased L-PHA signal (Fig.
402 S4D), indicating that NAGK deficiency results in altered glycosylation within tumors. This could
403 possibly reflect either elevated de novo synthesis in the small tumors that form or differences in
404 cellular composition. For example, activated fibroblast marker α-smooth muscle actin (α-SMA)
405 was more abundant in the NAGK KO tumors (Fig S4D). Residual NAGK signal in whole tumors
406 also presumably reflects expression in other cell types (Fig. S4D), since NAGK was
407 undetectable in the clonal cell lines used for injections (Fig. S3.1B). Taken together, these data
408 are consistent with the notion that NAGK is dispensable when nutrients are abundant but

409 becomes more important as the tumors outgrow their original nutrient supply and become more
410 dependent on scavenging and recycling and indicate that NAGK-mediated hexosamine salvage
411 supports tumor growth *in vivo*.

412

413 **DISCUSSION**

414 In this study, we identify a key role for NAGK in salvaging GlcNAc for UDP-GlcNAc synthesis
415 in PDA cells. We show that glutamine deprivation suppresses *de novo* hexosamine
416 biosynthesis, which is reciprocally increased upon NAGK deletion. Glutamine deprivation also
417 results in increased availability of GlcNAc for salvage. *NAGK* expression is elevated in human
418 PDA tumors, and NAGK deficiency suppresses GlcNAc salvage in cells and tumor growth in
419 mice.

420 This work raises several key questions for future investigation. First, the sources of GlcNAc
421 salvaged by NAGK remain to be fully elucidated. GlcNAc may be derived from recycling of
422 GlcNAc following O-GlcNAc removal or breakdown of glycoconjugates. Additionally, GlcNAc
423 may be recovered from the environment. Nutrient scavenging via macropinocytosis is a key
424 feature of PDA (Commisso et al., 2013; Kamphorst et al., 2015). Macropinocytosis has mostly
425 been associated with scavenging of protein to recover amino acids, but lysosomal break down
426 of glycoproteins may also release sugars including GlcNAc. Additionally, ECM components,
427 including hyaluronic acid (HA), which is a polymer of GlcNAc and glucuronic acid disaccharide
428 units, may be additional sources of GlcNAc for salvage in the tumor microenvironment. Indeed,
429 in a manuscript co-submitted with this one, Kim, Halbrook, and colleagues identify HA as a
430 major source of scavenged GlcNAc (Kim et al., 2020). Our manuscript and the Kim, Halbrook et

This manuscript has been co-submitted with Kim et al. (2020), "Pancreatic Cancers Scavenge Hyaluronic Acid to Support Growth."

431 al manuscript together indicate that NAGK may take on a heightened importance in the context
432 of high GlcNAc availability and nutrient deprivation, a situation that is likely to occur within the
433 tumor microenvironment.

434 Further, the key fates of UDP-GlcNAc that support tumor growth remain to be elucidated.
435 Sufficient UDP-GlcNAc is required for protein glycosylation to maintain homeostasis and
436 prevent ER stress, particularly in a rapidly dividing cell. Additionally, a wide range of cancers
437 exhibit elevated O-GlcNAc, which could contribute to driving pro-tumorigenic transcriptional and
438 signaling programs. In PDA specifically, the glycan CA19-9 is currently used as a biomarker for
439 disease progression and recent studies point to a functional role for CA19-9 in tumorigenesis
440 (Engle et al., 2019). UDP-GlcNAc is also required for HA synthesis, which is present in low
441 amounts in normal pancreas but increases in PanIN lesions and PDA (Provenzano et al., 2012).
442 PDA cells are capable of producing HA in vitro (Mahlbacher et al., 1992). Depletion of
443 fibroblasts in an autochthonous PDA mouse model results in a decrease in collagen I but not
444 HA in the tumor microenvironment, indicating that HA must be generated by another cell type,
445 possibly the tumor cells themselves (Özdemir et al., 2014). Previous studies demonstrated that
446 treatment of PDA with exogenous hyaluronidase can increase vascularization and improve drug
447 delivery to the tumor (Jacobetz et al., 2013; Provenzano et al., 2012), although a phase III
448 clinical trial reported no improvement in overall patient survival when combining pegylated
449 hyaluronidase with nab-paclitaxel plus gemcitabine (Cutsem et al., 2020). Recently, it was
450 shown that inhibiting the HBP by treatment with 6-diazo-5-oxo-l-norleucine (DON) depletes HA
451 and collagen in an orthotopic mouse model. DON treatment also increased CD8 T-cell
452 infiltration into the tumor, sensitizing the tumor to anti-PD1 therapy (Sharma et al., 2020). Thus,
453 targeting the HBP holds promise for improving the efficacy of other therapeutics. The findings of
454 the current study suggest that in addition to de novo hexosamine synthesis, targeting of

455 hexosamine salvage warrants further investigation in terms of potential for therapeutic
456 intervention. Of note, an inhibitor targeting PGM3, which converts GlcNAc-6-P to GlcNAc-1-P
457 and is thus required for both de novo UDP-GlcNAc synthesis and GlcNAc recycling, showed
458 efficacy in treating gemcitabine-resistant patient-derived xenograft PDA models (Ricciardiello et
459 al., 2020), as well as in breast cancer xenografts (Ricciardiello et al., 2018).

460 Finally, almost nothing is currently known about the role of NAGK and GlcNAc salvage in
461 normal physiology. Even in non-cancerous IL-3-dependent hematopoietic cells, a substantial
462 proportion of the UDP-GlcNAc pool remains unlabeled from ^{13}C-glucose (Wellen et al., 2010),
463 suggesting that salvage may contribute to UDP-GlcNAc pools in a variety of cell types.
464 However, while GFPT1 is required for embryonic development in mice, NAGK knockout mouse
465 embryos are viable (Dickinson et al., 2016). NAGK deficiency has not yet been characterized in
466 postnatal or adult mice. Perhaps GlcNAc salvage is dispensable when nutrients are available
467 and cells are not dividing, as in most healthy tissues. However, in a tumor, in which cells are
468 proliferating and nutrients are spread thin, NAGK and GlcNAc salvage may become more
469 important in feeding UDP-GlcNAc pools. Related questions include elucidating the mechanisms
470 regulating NAGK gene expression and putative post-translational modification, as well as
471 understanding the role of GALK2 in hexosamine salvage.

472 In sum, we report a key role for NAGK in feeding UDP-GlcNAc pools in PDA cells and in
473 supporting xenograft tumor growth. Further investigation will be needed to elucidate the
474 physiological functions of NAGK, as well as the mechanisms through which it supports tumor
475 growth and its potential role in modulating therapeutic responses.

476 **Funding Sources**: This work was supported by R01CA174761 and R01CA228339 to K.E.W.
477 This work was also funded in part under a grant with the Pennsylvania Department of Health to

This manuscript has been co-submitted with Kim et al. (2020), "Pancreatic Cancers Scavenge Hyaluronic Acid to Support Growth."

478 K.E.W. and I.A.B. The Department specifically disclaims responsibility for any analyses,
479 interpretations, or conclusions. I.A.B. acknowledges support of NIH Grants P30ES013508 and
480 P30CA016520. J.B. acknowledges support of NIH Grant R01CA046595. S.L.C. received
481 support from T32CA115299 and F31CA217070, as well as from a Patel Family Scholar Award.
482 H.A. was supported by post-doctoral fellowship K00CA212455. T.T. is supported by the
483 National Cancer Institute through pre-doctoral fellowship F31CA243294 and acknowledges the
484 Blavatnik Family for a predoctoral fellowship. L.I. is supported by T32 GM-07229 and T32
485 CA115299. S.T. is supported by the American Diabetes Association through post-doctoral
486 fellowship 1-18-PDF-144. Funding sources were not involved in study design, data collection
487 and interpretation, or the decision to submit the work for publication.

488 **Conflict of interest**: I.A.B. is a founder of Proteoform Bio and a paid consultant for Calico,
489 Chimerix, PTC Therapeutics, Takeda Pharmaceuticals, and Vivo Capital.

490 **References**

491 Akella, N.M., Ciraku, L., and Reginato, M.J. (2019). Fueling the fire: Emerging role of the
492 hexosamine biosynthetic pathway in cancer. BMC Biol. *17*, 1–14.

493 Caldwell, S.A., Jackson, S.R., Shahriari, K.S., Lynch, T.P., Sethi, G., Walker, S., Vosseller, K.,
494 and Reginato, M.J. (2010). Nutrient sensor O-GlcNAc transferase regulates breast cancer
495 tumorigenesis through targeting of the oncogenic transcription factor FoxM1. Oncogene *29*,
496 2831–2842.

497 Chen, R., Lai, L.A., Sullivan, Y., Wong, M., Wang, L., Riddell, J., Jung, L., Pillarisetty, V.G.,
498 Brentnall, T.A., and Pan, S. (2017). Disrupting glutamine metabolic pathways to sensitize
499 gemcitabine-resistant pancreatic cancer. Sci. Rep. *7*, 1–14.

This manuscript has been co-submitted with Kim et al. (2020), "Pancreatic Cancers Scavenge Hyaluronic Acid to Support Growth."

500 Commisso, C., Davidson, S.M., Soydaner-Azeloglu, R.G., Parker, S.J., Kamphorst, J.J.,
501 Hackett, S., Grabocka, E., Nofal, M., Drebin, J.A., Thompson, C.B., et al. (2013).
502 Macropinocytosis of protein is an amino acid supply route in Ras-transformed cells. Nature *497*,
503 633–637.

504 Cutsem, E. Van, Tempero, M.A., Sigal, D., Oh, D., Fazio, N., Macarulla, T., Hitre, E., Hammel,
505 P., Hendifar, A., Bates, S., et al. (2020). Randomized Phase III Trial of Pegvorhyaluronidase
506 Alfa With Nab-Paclitaxel Plus Gemcitabine for Patients With Hyaluronan-High Metastatic
507 Pancreatic Adenocarcinoma abstract. J. Clin. Oncol.

508 Denzel, M.S., and Antebi, A. (2015). Hexosamine pathway and (ER) protein quality control.
509 Curr. Opin. Cell Biol. *33*, 14–18.

510 Dickinson, M.E., Flenniken, A.M., Ji, X., Teboul, L., Wong, M.D., White, J.K., Meehan, T.F.,
511 Weninger, W.J., Westerberg, H., Adissu, H., et al. (2016). High-throughput discovery of novel
512 developmental phenotypes. Nature *537*, 508–514.

513 Doench, J.G., Fusi, N., Sullender, M., Hegde, M., Vaimberg, E.W., Donovan, K.F., Smith, I.,
514 Tothova, Z., Wilen, C., Orchard, R., et al. (2016). Optimized sgRNA design to maximize activity
515 and minimize off-target effects of CRISPR-Cas9. Nat. Biotechnol. *34*, 184–191.

516 Edgar, R., Domrachev, M., and Lash, A.E. (2002). Gene Expression Omnibus: NCBI gene
517 expression and hybridization array data repository. Nucleic Acids Res. *30*, 207–210.

518 Engle, D.D., Tiriac, H., Rivera, K.D., Pommier, A., Oni, T.E., Alagesan, B., Lee, E.J., Yao, M.A.,
519 Lucito, M.S., Spielman, B., et al. (2019). The Glycan CA19-9 Promotes Pancreatitis and
520 Pancreatic Cancer in Mice. *364*, 1156–1162.

This manuscript has been co-submitted with Kim et al. (2020), “Pancreatic Cancers Scavenge Hyaluronic Acid to Support Growth.”

521 Ferrer, C.M., Lu, T.Y., Bacigalupa, Z.A., Katsetos, C.D., Sinclair, D.A., and Reginato, M.J.
522 (2017). O-GlcNAcylation regulates breast cancer metastasis via SIRT1 modulation of FOXM1
523 pathway. Oncogene *36*, 559–569.

524 Granovsky, M., Fata, J., Pawling, J., Muller, W.J., Khokha, R., and Dennis, J.W. (2000).
525 Suppression of tumor growth and metastasis in Mgat5-deficient mice. Nat. Med. *6*, 306–312.

526 Gu, Y., Mi, W., Ge, Y., Liu, H., Fan, Q., Han, C., Yang, J., Han, F., Lu, X., and Yu, W. (2010).
527 GlcNAcylation plays an essential role in breast cancer metastasis. Cancer Res. *70*, 6344–6351.

528 Guillaumond, F., Leca, J., Olivares, O., Lavaut, M.-N.N., Vidal, N., Berthezène, P., Dusetti, N.J.,
529 Loncle, C., Calvo, E., Turrini, O., et al. (2013). Strengthened glycolysis under hypoxia supports
530 tumor symbiosis and hexosamine biosynthesis in pancreatic adenocarcinoma. Proc. Natl. Acad.
531 Sci. U. S. A. *110*, 3919–3924.

532 Guo, H., Zhang, B., Nairn, A. V., Nagy, T., Moremen, K.W., Buckhaults, P., and Pierce, M.
533 (2017). O-Linked N-Acetylglucosamine (O-GlcNAc) Expression Levels Epigenetically Regulate
534 Colon Cancer Tumorigenesis by Affecting the Cancer Stem Cell Compartment via Modulating
535 Expression of Transcriptional Factor MYBL1. J. Biol. Chem. *292*, 4123–4137.

536 Guo, J.Y., Chen, H.Y., Mathew, R., Fan, J., Strohecker, A.M., Karsli-Uzunbas, G., Kamphorst,
537 J.J., Chen, G., Lemons, J.M.S., Karantza, V., et al. (2011). Activated Ras requires autophagy to
538 maintain oxidative metabolism and tumorigenesis. Genes Dev. *25*, 460–470.

539 Guo, L., Worth, A.J., Mesaros, C., Snyder, N.W., Jerry, D., and Blair, I.A. (2016).
540 Diisopropylethylamine/hexafluoroisopropanol-mediated ion- pairing UHPLC-MS for phosphate
541 and carboxylate metabolite analysis: utility for studying cellular metabolism. Rapid Commun
542 Mass Spectrom. *30*, 1835–1845.

This manuscript has been co-submitted with Kim et al. (2020), “Pancreatic Cancers Scavenge Hyaluronic Acid to Support Growth.”

543 Halbrook, C.J., and Lyssiotis, C.A. (2017). Employing Metabolism to Improve the Diagnosis and
544 Treatment of Pancreatic Cancer. Cancer Cell *31*, 5–19.

545 Housley, M.P., Rodgers, J.T., Udeshi, N.D., Kelly, T.J., Shabanowitz, J., Hunt, D.F., Puigserver,
546 P., and Hart, G.W. (2008). O-GlcNAc regulates FoxO activation in response to glucose. J. Biol.
547 Chem. *283*, 16283–16292.

548 Jacobetz, M.A., Chan, D.S., Neesse, A., Bapiro, T.E., Cook, N., Frese, K.K., Feig, C.,
549 Nakagawa, T., Caldwell, M.E., Zecchini, H.I., et al. (2013). Hyaluronan impairs vascular function
550 and drug delivery in a mouse model of pancreatic cancer. Gut *62*, 112–120.

551 Kamphorst, J.J., Nofal, M., Commisso, C., Hackett, S.R., Lu, W., Grabocka, E., Vander Heiden,
552 M.G., Miller, G., Drebin, J.A., Bar-Sagi, D., et al. (2015). Human Pancreatic Cancer Tumors Are
553 Nutrient Poor and Tumor Cells Actively Scavenge Extracellular Protein. Cancer Res. *75*, 544–
554 553.

555 Kim, P.K., Halbrook, C.J., Kerk, S.A., Wisner, S., Kremer, D., Sajjakulnukit, P., Hou, S.W.,
556 Thurston, G., Anand, A., Yan, L., et al. (2020). Hyaluronic Acid Fuels Pancreatic Cancer
557 Growth. BioRxiv.

558 Lau, K.S., Partridge, E.A., Grigorian, A., Silvescu, C.I., Reinhold, V.N., Demetriou, M., and
559 Dennis, J.W. (2007). Complex N-Glycan Number and Degree of Branching Cooperate to
560 Regulate Cell Proliferation and Differentiation. Cell *129*, 123–134.

561 Li, D., Li, Y., Wu, X., Li, Q., Yu, J., Gen, J., and Zhang, X.-L. (2008). Knockdown of Mgat5
562 Inhibits Breast Cancer Cell Growth with Activation of CD4 + T Cells and Macrophages . J.
563 Immunol. *180*, 3158–3165.

This manuscript has been co-submitted with Kim et al. (2020), "Pancreatic Cancers Scavenge Hyaluronic Acid to Support Growth."

564 Lynch, T.P., Ferrer, C.M., Jackson, S.R.E., Shahriari, K.S., Vosseller, K., and Reginato, M.J.
565 (2012). Critical role of O-linked β-N-acetylglucosamine transferase in prostate cancer invasion,
566 angiogenesis, and metastasis. J. Biol. Chem. *287*, 11070–11081.

567 Lyssiotis, C.A., and Kimmelman, A.C. (2017). Metabolic Interactions in the Tumor
568 Microenvironment. Trends Cell Biol. *27*, 863–875.

569 Mahlbacher, V., Sewing, A., Elsässer, H.P., and Kern, H.F. (1992). Hyaluronan is a secretory
570 product of human pancreatic adenocarcinoma cells. Eur. J. Cell Biol. *58*, 28—34.

571 Mereiter, S., Balmaña, M., Campos, D., Gomes, J., and Reis, C.A. (2019). Glycosylation in the
572 Era of Cancer-Targeted Therapy: Where Are We Heading? Cancer Cell *36*, 6–16.

573 Moloughney, J.G.G., Kim, P.K.K., Vega-cotto, N.M.M., Wu, C.-C., Zhang, S., Adlam, M., Lynch,
574 T., Chou, P.-C., Rabinowitz, J.D.D., Werlen, G., et al. (2016). mTORC2 Responds to Glutamine
575 Catabolite Levels to Modulate the Hexosamine Biosynthesis Enzyme GFAT1. Mol. Cell *63*,
576 811–826.

577 Moseley, H.N.B., Lane, A.N., Belshoff, A.C., Higashi, R.M., and Fan, T.W.M. (2011). A novel
578 deconvolution method for modeling UDP-N-acetyl-D-glucosamine biosynthetic pathways based
579 on 13C mass isotopologue profiles under non-steady-state conditions. BMC Biol. *9*.

580 Munkley, J. (2019). The glycosylation landscape of pancreatic cancer (Review). Oncol. Lett. *17*,
581 2569–2575.

582 Özdemir, B.C., Pentcheva-Hoang, T., Carstens, J.L., Zheng, X., Wu, C.C., Simpson, T.R.,
583 Laklai, H., Sugimoto, H., Kahlert, C., Novitskiy, S. V., et al. (2014). Depletion of carcinoma-
584 associated fibroblasts and fibrosis induces immunosuppression and accelerates pancreas

585 cancer with reduced survival. Cancer Cell *25*, 719–734.

586 Park, S.Y., Kim, H.S., Kim, N.H., Ji, S., Cha, S.Y., Kang, J.G., Ota, I., Shimada, K., Konishi, N.,
587 Nam, H.W., et al. (2010). Snail1 is stabilized by O-GlcNAc modification in hyperglycaemic
588 condition. EMBO J. *29*, 3787–3796.

589 Pei, H., Li, L., Fridley, B.L., Jenkins, G.D., Kalari, K.R., Lingle, W., Petersen, G., Lou, Z., and
590 Wang, L. (2009). FKBP51 Affects Cancer Cell Response to Chemotherapy by Negatively
591 Regulating Akt. Cancer Cell *16*, 259–266.

592 Provenzano, P.P., Cuevas, C., Chang, A.E., Goel, V.K., Von Hoff, D.D., and Hingorani, S.R.
593 (2012). Enzymatic Targeting of the Stroma Ablates Physical Barriers to Treatment of Pancreatic
594 Ductal Adenocarcinoma. Cancer Cell *21*, 418–429.

595 Rahib, L., Smith, B.D., Aizenberg, R., Rosenzweig, A.B., Fleshman, J.M., and Matrisian, L.M.
596 (2014). Projecting cancer incidence and deaths to 2030: The unexpected burden of thyroid,
597 liver, and pancreas cancers in the united states. Cancer Res. *74*, 2913–2921.

598 Ricciardiello, F., Votta, G., Palorini, R., Raccagni, I., Brunelli, L., Paiotta, A., Tinelli, F., D'Orazio,
599 G., Valtorta, S., De Gioia, L., et al. (2018). Inhibition of the Hexosamine Biosynthetic Pathway
600 by targeting PGM3 causes breast cancer growth arrest and apoptosis. Cell Death Dis. *9*.

601 Ricciardiello, F., Gang, Y., Palorini, R., Li, Q., Giampà, M., Zhao, F., You, L., La Ferla, B., De
602 Vitto, H., Guan, W., et al. (2020). Hexosamine pathway inhibition overcomes pancreatic cancer
603 resistance to gemcitabine through unfolded protein response and EGFR-Akt pathway
604 modulation. Oncogene 4103–4117.

605 Ryczko, M.C., Pawling, J., Chen, R., Abdel Rahman, A.M., Yau, K., Copeland, J.K., Zhang, C.,

606 Surendra, A., Guttman, D.S., Figeys, D., et al. (2016). Metabolic Reprogramming by
607 Hexosamine Biosynthetic and Golgi N-Glycan Branching Pathways. Sci. Rep. *6*, 23043.

608 Sanjana, N.E., Shalem, O., and Zhang, F. (2014). Sanjana, Shalem et Zhang. Nat. Med. *11*,
609 783–784.

610 Schneider, C.A., Rasband, W.S., and Eliceiri, K.W. (2012). NIH Image to ImageJ: 25 years of
611 image analysis. Nat. Methods *9*, 671–675.

612 Sharma, N.S., Saluja, A., Banerjee, S., Sharma, N.S., Gupta, V.K., Garrido, V.T., Hadad, R.,
613 Durden, B.C., Kesh, K., Giri, B., et al. (2020). Targeting tumor-intrinsic hexosamine biosynthesis
614 sensitizes pancreatic cancer to anti-PD1 therapy Graphical abstract Find the latest version :
615 Targeting tumor-intrinsic hexosamine biosynthesis sensitizes pancreatic cancer to anti-PD1
616 therapy. *130*, 451–465.

617 Steenackers, A., Olivier-Van Stichelen, S., Baldini, S.F., Dehennaut, V., Toillon, R.A., Le
618 Bourhis, X., El Yazidi-Belkoura, I., and Lefebvre, T. (2016). Silencing the nucleocytoplasmic O-
619 GlcNAc transferase reduces proliferation, adhesion, and migration of cancer and fetal human
620 colon cell lines. Front. Endocrinol. (Lausanne). *7*, 1–11.

621 Swamy, M., Pathak, S., Grzes, K.M., Damerow, S., Sinclair, L. V, van Aalten, D.M.F., and
622 Cantrell, D.A. (2016). Glucose and glutamine fuel protein O-GlcNAcylation to control T cell self-
623 renewal and malignancy. Nat. Immunol. *17*, 1–11.

624 Tang, Z., Kang, B., Li, C., Chen, T., and Zhang, Z. (2019). GEPIA2: an enhanced web server for
625 large-scale expression profiling and interactive analysis. Nucleic Acids Res. *47*, W556–W560.

626 Taylor, R.P., Parker, G.J., Hazel, M.W., Soesanto, Y., Fuller, W., Yazzie, M.J., and McClain,

627 D.A. (2008). Glucose deprivation stimulates O-GlcNAc modification of proteins through up-
628 regulation of O-linked N-acetylglucosaminyltransferase. J. Biol. Chem. *283*, 6050–6057.

629 Trefely, S., Ashwell, P., and Snyder, N.W. (2016). FluxFix: Automatic isotopologue
630 normalization for metabolic tracer analysis. BMC Bioinformatics *17*, 1–8.

631 Wellen, K.E., Lu, C., Mancuso, A., Lemons, J.M.S.S., Ryczko, M., Dennis, J.W., Rabinowitz,
632 J.D., Coller, H.A., and Thompson, C.B. (2010). The hexosamine biosynthetic pathway couples
633 growth factor-induced glutamine uptake to glucose metabolism. Genes Dev. *24*, 2784–2799.

634 Wyant, G.A., Abu-Remaileh, M., Frenkel, E.M., Laqtom, N.N., Dharamdasani, V., Lewis, C.A.,
635 Chan, S.H., Heinze, I., Ori, A., and Sabatini, D.M. (2018). NUFIP1 is a ribosome receptor for
636 starvation-induced ribophagy. Science (80-.). *360*, 751–758.

637 Ying, H., Kimmelman, A.C., Lyssiotis, C.A., Hua, S., Chu, G.C., Fletcher-Sananikone, E.,
638 Locasale, J.W., Son, J., Zhang, H., Coloff, J.L., et al. (2012). Oncogenic kras maintains
639 pancreatic tumors through regulation of anabolic glucose metabolism. Cell *149*, 656–670.

640 Zhou, X., Chen, H., Wang, Q., Zhang, L., and Zhao, J. (2011). Knockdown of Mgat5 inhibits
641 CD133+ human pulmonary adenocarcinoma cell growth in vitro and in vivo. Clin. Invest. Med.
642 *34*, E155-62.

643

644

This manuscript has been co-submitted with Kim et al. (2020), “Pancreatic Cancers Scavenge Hyaluronic Acid to Support Growth.”

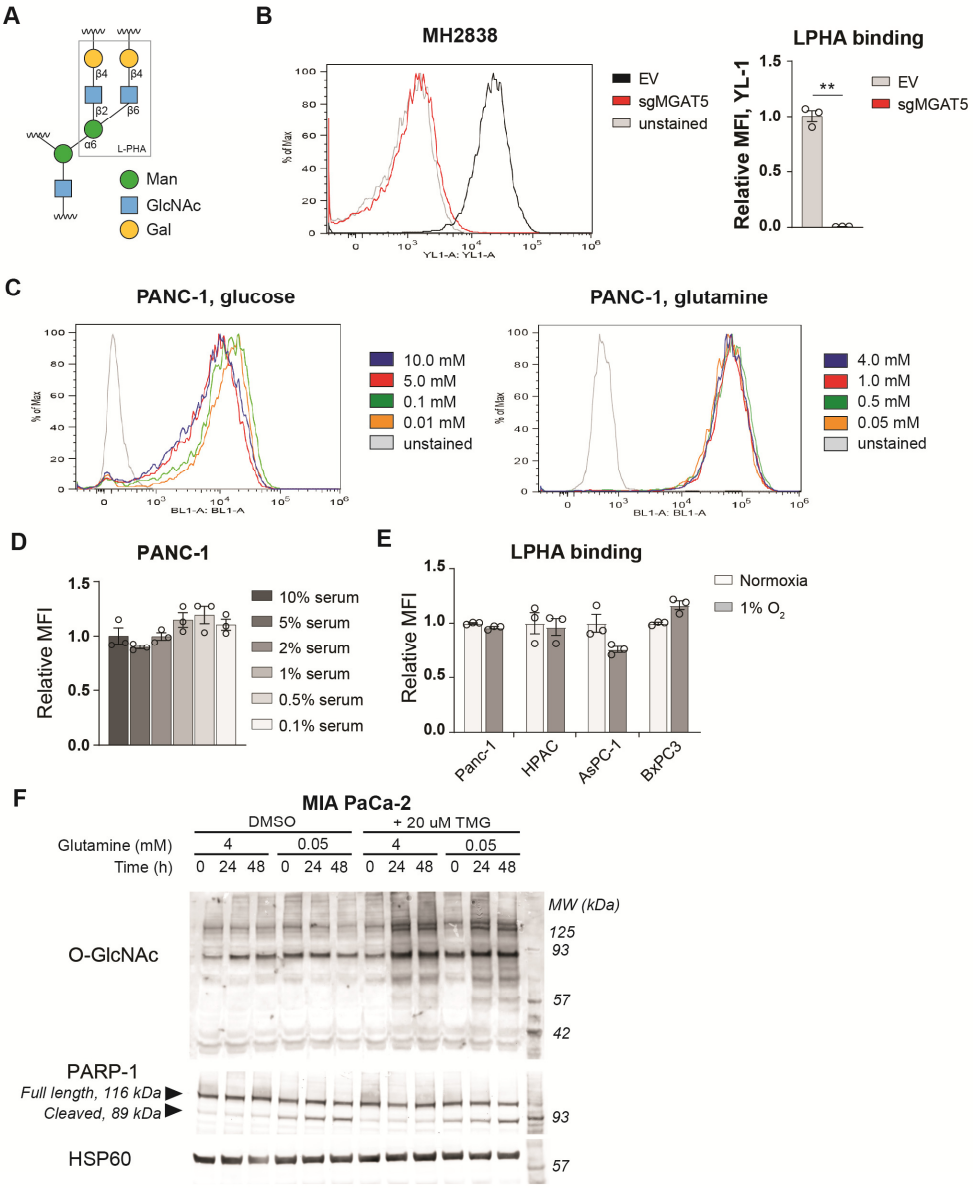

Supplemental Figure 1: LPHA binding detects MGAT5-dependent glycans.
A) Diagram of LPHA binding. LPHA recognizes specifically the β1-6 linkage established by MGAT5. **B)** LPHA binding on MGAT5 knockout cells isolated from a KPCY tumor (Li, Byrne et al., 2018), representative flow plot and quantification. Graph shows MFI relative to control cells. Statistical significance was calculated by unpaired t-test. **C)** Representative flow plots for LPHA binding graphed in Fig. 1D, E on PANC-1 cells in low glucose and low glutamine. **D-E)** LPHA binding in PDA cells in low nutrients. Cells were incubated in the indicated concentrations of serum (D) or oxygen (E) for 48 hours and then analyzed by flow cytometry. Graph shows MFI relative to control condition. **F)** Western blot for O-GlcNAc and PARP in MIA PaCa-2 cells cultured in the indicated concentrations of glutamine with or without TMG for the indicated time. Statistical significance was calculated by one-way ANOVA (D) and unpaired t-test (E). Panels B) - E) are representative of at least two independent experimental replicates. *, $p \leq 0.05$; **, $p \leq 0.01$; **, $p \leq 0.001$.

This manuscript has been co-submitted with Kim et al. (2020), “Pancreatic Cancers Scavenge Hyaluronic Acid to Support Growth.”

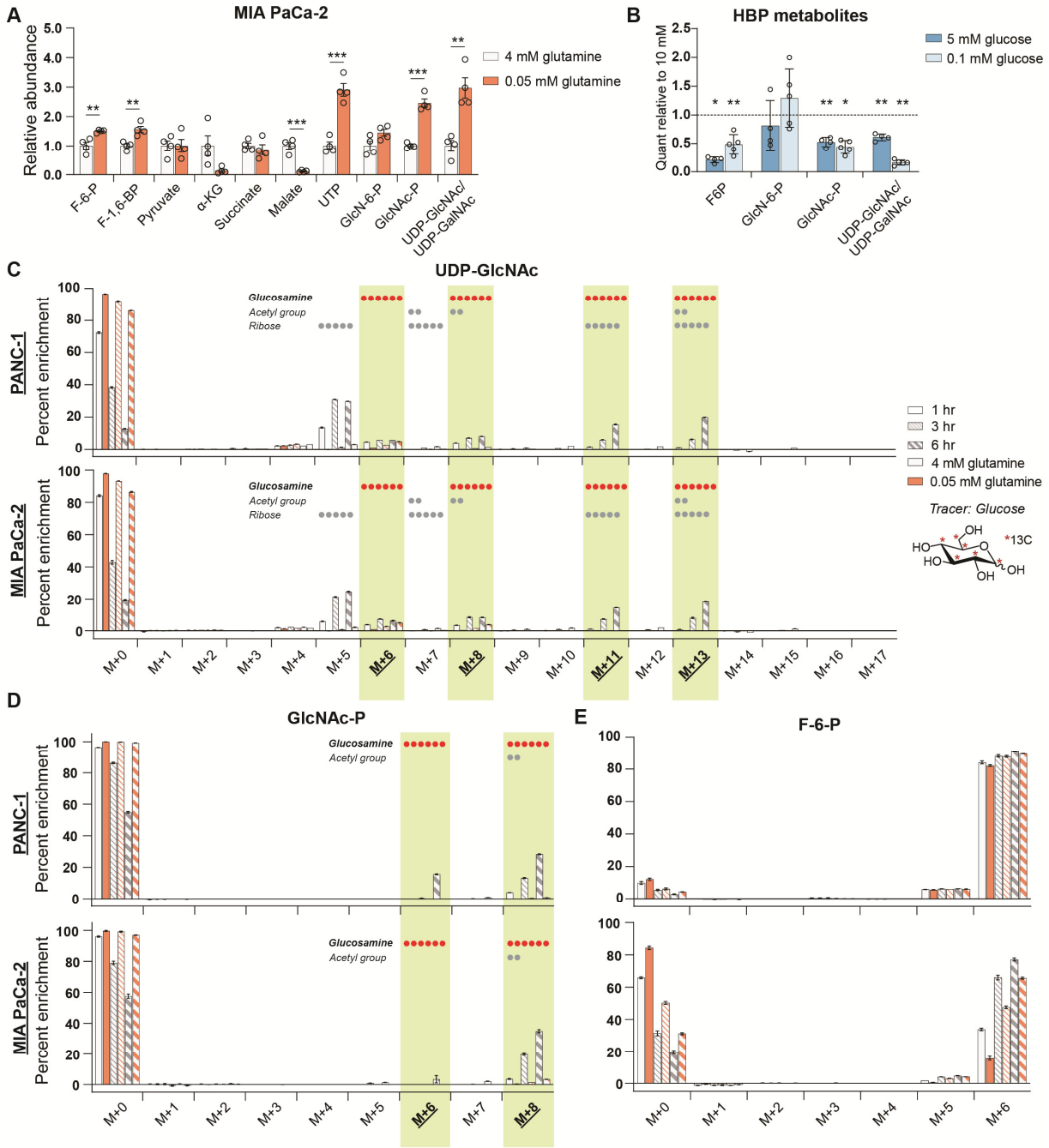

Supplemental Figure S2.1: De novo hexosamine synthesis is suppressed in low glutamine conditions.
A) Metabolite measurements in MIA PaCa-2 cells after culture for 48 hours in 0.05 mM glutamine. Quantification is normalized to 4 mM glutamine condition. Statistical significance was calculated by unpaired t-test. Mean +/- SEM of four biological replicates is represented. **B)** Measurement of HBP metabolites in PANC-1 cells after culture for 48 hours in 5 mM or 0.1 mM glucose. Mean +/- SEM of four (5 mM) or five (0.1 mM) biological replicates is represented. Statistical significance was calculated by unpaired t-test comparing each low glucose condition to the 10 mM glucose control in each experiment. **C)** Measurement of 13C glucose incorporation into UDP-GlcNAc in high and low glutamine. Mean +/- SEM of three biological replicates is represented. **D)** Measurement of 13C glucose incorporation into GlcNAc-P in high and low glutamine. Mean +/- SEM of three biological replicates is represented. For (C-D), components of molecule labeled in each isotopologue are indicated, with dots representing the number of carbons; highlighted panels identify glucosamine ring labeling. **E)** Measurement of 13C glucose into fructose-6-phosphate in high and low glutamine. Mean +/- SEM of three biological replicates is represented. *, $p \leq 0.05$; **, $p \leq 0.01$; ***, $p \leq 0.001$.

647

648 This manuscript has been co-submitted with Kim et al. (2020), “Pancreatic Cancers Scavenge Hyaluronic Acid to Support Growth.”

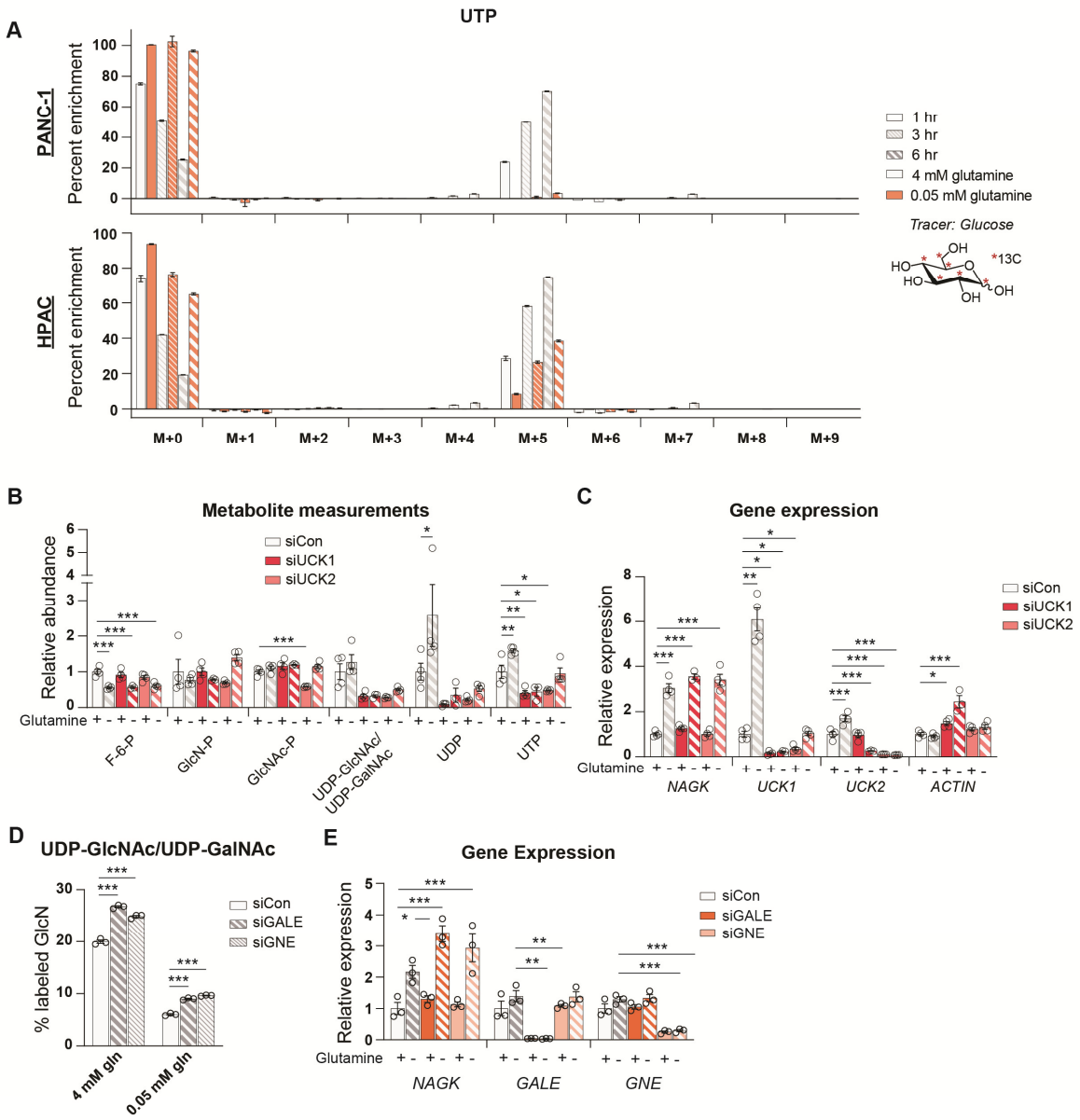

Supplemental Figure S2.2: Uridine is salvaged in glutamine restricted conditions.
A) Measurement of incorporation of 13C glucose into uridine triphosphate (UTP) in high and low glutamine. Mean +/- SEM of three biological replicates is represented. **B)** Measurement of metabolites in PANC-1 cells after transfection with the indicated siRNAs and incubation in 4 mM (+) or 0.05 mM (-) glutamine for 48 hours. Mean +/- SEM of four biological replicates is represented. **C)** Gene expression of the indicated genes in PANC-1 cells after transfection with the indicated siRNAs and incubation in 4 mM (+) or 0.05 mM (-) glutamine for 48 hours. Mean +/- SEM of four biological replicates is represented. **D)** Measurement of incorporation of 13C glucose into UDP-GlcNAc in PANC-1 cells transfected with the indicated siRNAs and incubated in 4 mM or 0.05 mM glutamine for 48 hours. Mean +/- SEM of three biological replicates is represented. **E)** Gene expression of the indicated genes in PANC-1 cells after transfection with the indicated siRNAs and incubation in 4 mM (+) or 0.05 (-)mM glutamine for 48 hours. Mean +/- SEM of three biological replicates is represented. *, $p \leq 0.05$; **, $p \leq 0.01$; ***, $p \leq 0.001$.

This manuscript has been co-submitted with Kim et al. (2020), “Pancreatic Cancers Scavenge Hyaluronic Acid to Support Growth.”

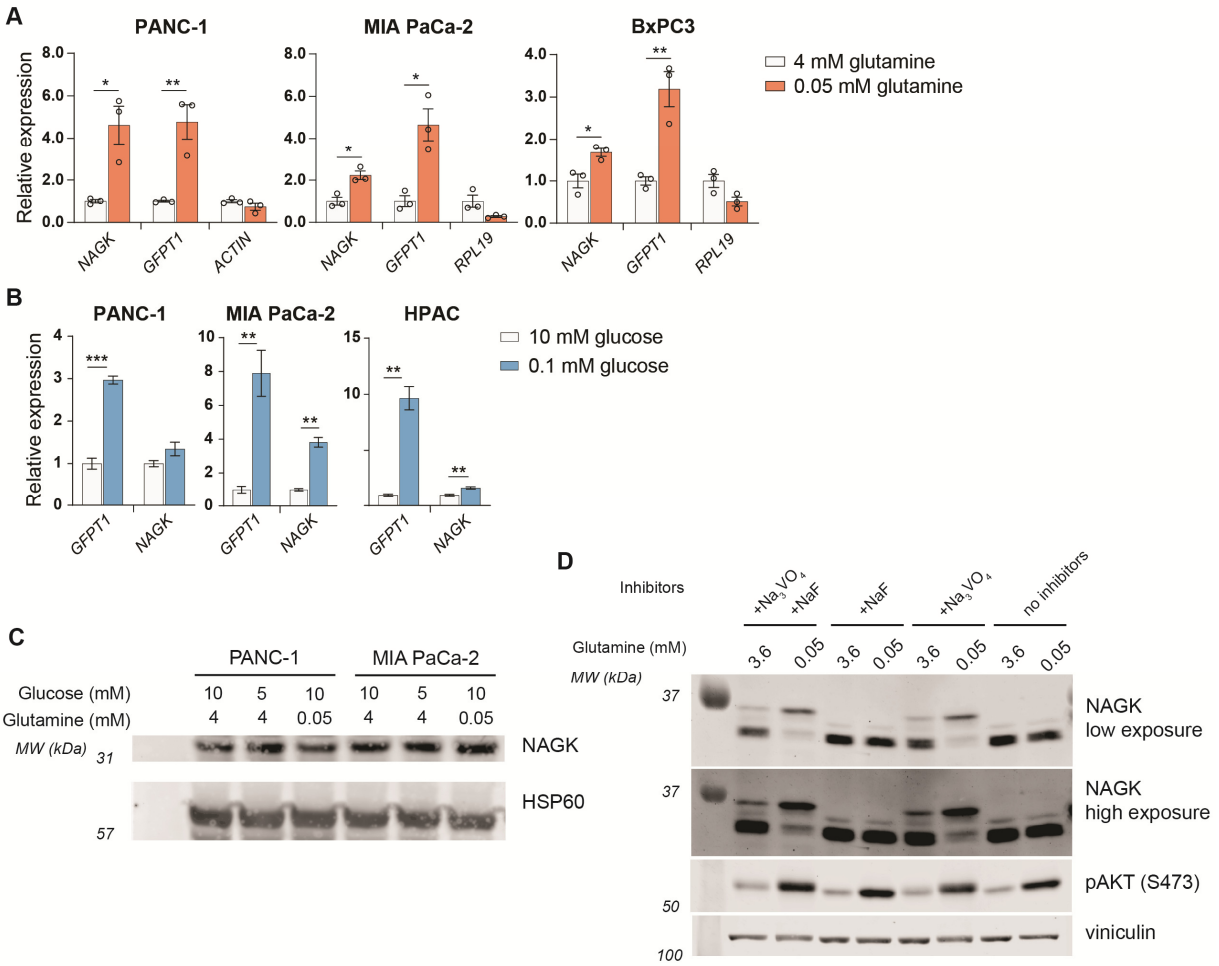

Supplemental Figure S2.3: NAGK protein expression does not increase in low glutamine despite increase in NAGK gene expression. **A)** Gene expression of the indicated genes in PDA cell lines after incubation in 4 mM or 0.05 mM glutamine for 48 hours. Mean +/- SEM of three biological replicates is represented. Statistical significance was determined by unpaired t-test. **B)** Gene expression of the indicated genes in PDA cell lines after incubation in 10 mM or 0.1 mM glucose for 48 hours. Mean +/- SEM of three biological replicates is represented. Statistical significance was determined by unpaired t-test. **C)** Western blot for NAGK in low nutrient conditions. PANC-1 and MIA PaCa-2 cells were cultured in the indicated concentrations of glucose and glutamine for 48 hours. **D)** Western blot for NAGK in low nutrient conditions. PANC-1 cells were cultured in the indicated glutamine concentrations and lysates were prepared with or without phosphatase inhibitors. A band shift is observed for NAGK in lysates with Na_3VO_4. *, $p \leq 0.05$; **, $p \leq 0.01$; ***, $p \leq 0.001$.

This manuscript has been co-submitted with Kim et al. (2020), “Pancreatic Cancers Scavenge Hyaluronic Acid to Support Growth.”

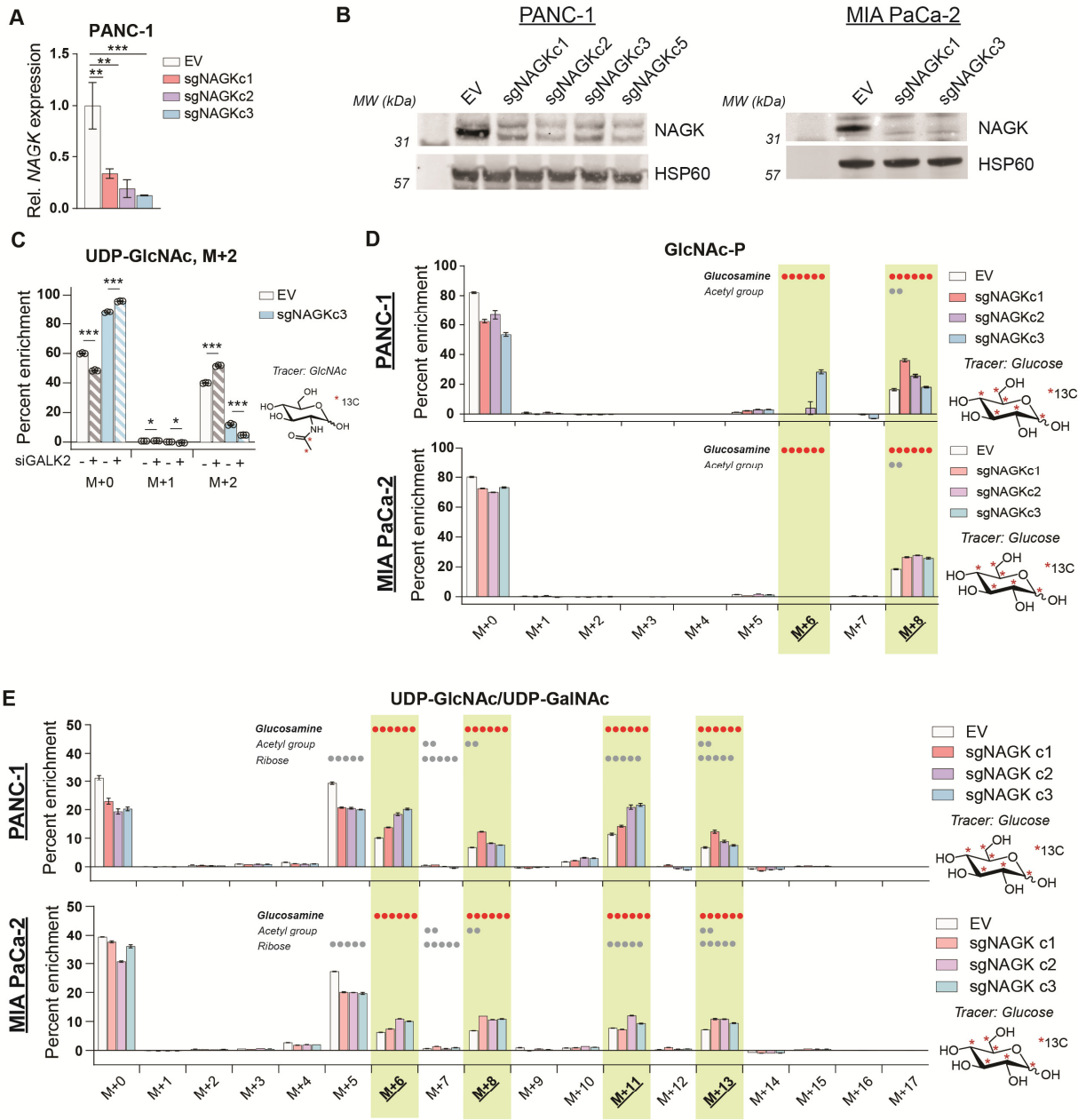

Supplemental Figure S3.1: NAGK knockout cells show increased enrichment of 13C glucose into hexosamine intermediates.
A) Gene expression of NAGK in PANC-1 NAGK CRISPR cells. Mean +/- SEM of three biological replicates is represented. Statistical significance was determined by one-way ANOVA. **B)** Western blot for NAGK and HSP60 in PANC-1 (left) and MIA PaCa-2 (right) NAGK CRISPR knockout cells. **C)** Measurement of incorporation of 13C GlcNAc labeled on the acetyl group into UDP-GlcNAc in PANC-1 NAGK knockout cells. Cells were incubated with 10 mM 13C GlcNAc for 3 hours. Mean +/- SEM of three biological replicates is represented. Statistical significance was determined by unpaired t-test comparing siCon and siGALK2 for each clone. **D)** Measurement of incorporation of 13C glucose into GlcNAc-P in NAGK knockout cells. Mean +/- SEM of three biological replicates is represented. **E)** Measurement of incorporation of 13C glucose into UDP-GlcNAc in NAGK knockout cells. Mean +/- SEM of three biological replicates is represented. For (D-E), components of molecule labeled in each isotopologue are indicated, with dots representing the number of carbons; highlighted panels identify glucosamine ring labeling. *, $p \leq 0.05$; **, $p \leq 0.01$; ***, $p \leq 0.01$.

This manuscript has been co-submitted with Kim et al. (2020), “Pancreatic Cancers Scavenge Hyaluronic Acid to Support Growth.”

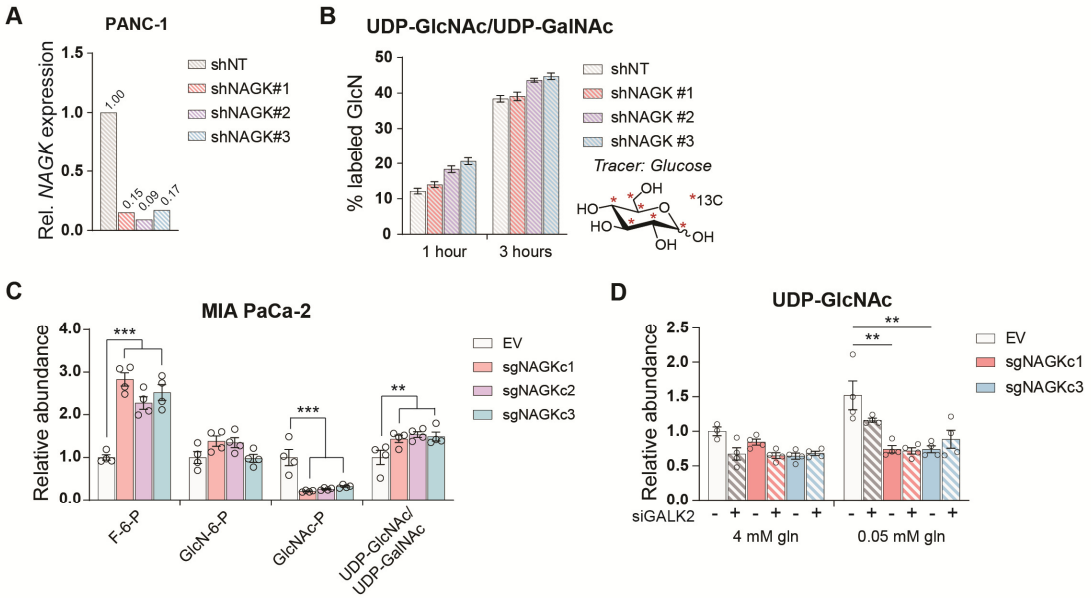

Supplementary Figure S3.2: HBP metabolites in NAGK KO cells.
A) Gene expression of NAGK in PANC-1 cells transfected with shRNA against NAGK. One biological sample is represented. **B)** Incorporation of 13C glucose into the glucosamine ring of UDP-GlcNAc in PANC-1 cells transfected with the indicated shRNAs targeting NAGK. Mean +/- SEM of three biological replicates is represented.**C)** Measurement of HBP metabolites in MIA PaCa-2 NAGK knockout cells cultured in 4 mM glutamine. Mean +/- SEM of four biological replicates is represented. Statistical significance was calculated by unpaired t-test comparing the mean of the three CRISPR clones and the empty vector control. **D)** Measurement of UDP-GlcNAc in PANC-1 NAGK knockout cells. Mean +/- SEM of four biological replicates is represented. Statistical significance was calculated by one-way ANOVA comparing each knockout to the EV control. *, $p \leq 0.05$; **, $p \leq 0.01$; ***, $p \leq 0.001$.

This manuscript has been co-submitted with Kim et al. (2020), “Pancreatic Cancers Scavenge Hyaluronic Acid to Support Growth.”

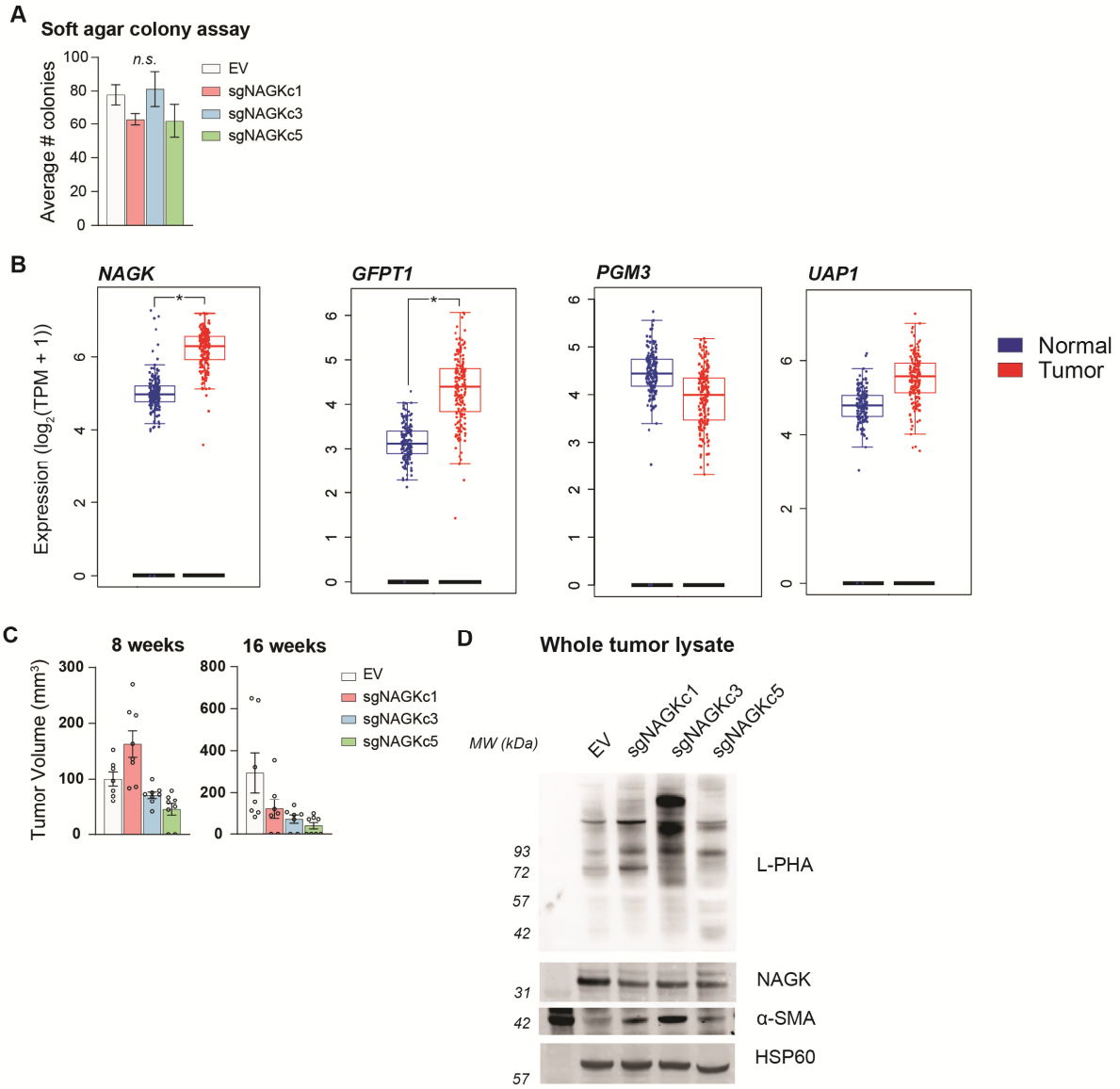

Supplementary Figure S4: NAGK knockout tumors show increased LPHA binding.
A) Soft agar colony formation in NAGK knockout and control cells. Mean +/- SEM of three biological replicates is represented. **B)** Gene expression data plotted using GEPIA2 comparing TCGA pancreatic cancer samples with TCGA normal pancreas samples and GTEx data. Differential analysis between tumor and normal tissues was analyzed by one-way ANOVA. *, $p < 0.05$. **C)** Tumor volume of NAGK knockout tumors at earlier time points in the experiment. Initial growth of NAGK knockout cells in vivo was comparable to control cells, but over time NAGK knockout tumors either stopped growing or regressed. **D)** Western blots for NAGK and α-SMA, and blot probed for LPHA binding, in whole tumor lysate samples. Blot for HSP60 as loading control.

This manuscript has been co-submitted with Kim et al. (2020), "Pancreatic Cancers Scavenge Hyaluronic Acid to Support Growth."